UNIVERSITA' DEGLI STUDI DI PADOVA
Dipartimento di Ingegneria Industriale
Corso di Laurea Magistrale in Ingegneria Aerospaziale

Tesi di Laurea Magistrale in
Ingegneria Aerospaziale

"Impact of environmental, instrumental and data processing parameters on the performance of the Radar for Icy Moon Exploration"

Relatore:
Prof. Enrico Lorenzini

Correlatori:
Prof. Lorenzo Bruzzone
Sanchari Thakur

Laureando:
Andrea Vettor

Anno Accademico 2018/2019

“Talvolta ci si perde in una direzione spirituale contraria alle nostre inclinazioni; per un certo tempo si lotta eroicamente contro la marea e il vento, e in fondo contro se stessi: ci si stanca, ci viene il fiato grosso; ciò che si compie non dà alcuna gioia, pensiamo di aver dovuto pagare troppo cari questi successi. Anzi si dispera della propria fecondità, del proprio futuro, forse già nel bel mezzo della vittoria. - Finalmente, finalmente si torna indietro - e adesso il vento soffia nella nostra vela e ci spinge sulla nostra rotta. Che felicità!”

F. W. Nietzsche, *“Umano, troppo umano”*

Abstract

Jupiter’s icy moons are one the most important targets for the search of habitable environments outside the Earth, due to their considerable water content both in liquid and solid state. Among the technologies that allow to characterize these planetary bodies, Radar Sounders (RSs) are the only instruments that can directly observe the subsurface. RSs are based on the transmission and successive recording of radio waves and are able to produce 2-D images (radargrams) of the subsurface, by leveraging the doppler shift induced in the recorded signal by the relative motion of the antenna and the target. A number of numerical techniques are proposed in literature to simulate RSs performance but they usually require high computational capabilities and strong assumptions on the investigated target. In this work we follow a recently proposed simulation approach that exploits the data available from existing RSs in geologically analogous terrains, to produce realistic simulations of the Ganymede’s targets that will be investigated by RIME (Radar for Icy Moon Exploration), the RS that is planned for launch in 2022 onboard JUICE (JUpiter Icy Moons Explorer). We first applied this methodology to the pre-processed radargram of a pedestal crater on Mars collected by SHARAD (SHAllow RADar), in order to evaluate the impact of geoelectrical and instrumental parameters variation on radargrams appearance. We then extended the approach to the raw data of the same target, in order to take into account the influence of the SAR (Synthetic Aperture Radar) focusing process. Besides providing a simulated radargrams database, which will be usufull for the training of automatic feature detection software, we performed preliminary interpretation of the simulated data, in terms of radargram similarity and interface detectability. The results confirm the potential of this approach to characterize the impact of geoelectrical, instrumental and data processing parameters variation on our ability to discriminate between different geoelectrical hypotheses and to detect subsurface structures.

Acknowledgments

First of all I would like to thank Prof. Enrico Lorenzini for encouraging me to undertake this experience and for the precious advice he has given me throughout my research period.

I am deeply grateful to Prof. Lorenzo Bruzzone, for welcoming me at the Remote Sensing Laboratory, and to Sanchari Thakur, for her constant support and endless patience. I would also like to thank Adamo Ferro, for his outstanding open source project and for helping me with the simulations, and Cristiano Gerardi, for graphical support.

Finally, I will never be able to sufficiently express my gratitude towards my family for their unconditional love.

Table of Contents

Introduction

Since their discovery in 1610, Galilean moons have represented one of the main goals of space exploration. A number of space missions have been sent to the Jupiter's satellites in order to investigate their geological features and infer important information about the origin and evolution of the Solar System.

Among the four natural satellites, Jupiter's icy moons (i.e. Ganymede, Europa and Callisto) have raised particular interest for their peculiar structure and their significant water content, both in liquid and solid state, making them one of the principal targets for the search of habitable environments outside the Earth.

Radar sounding is one of the techniques that seem to be able to guarantee the highest scientific return in this regard. Based on the transmission and successive recording of electromagnetic signals, radar sounders allow to remotely investigate geological features down to several kilometers beneath the surface by creating two-dimensional images . Due to the outstanding potential of this technology, radar sounding instruments will be featured by two missions scheduled to launch toward Jupiter's system in the near future, i.e. ESA's JUICE (Jupiter Icy Moons Explorer) and NASA's Europa Clipper.

The scope of this thesis is to help predict how different environmental, instrumental and data processing parameters will impact RIME's performance and to produce helpful guidelines for the operation management phase of the mission. For this purpose, an

approach based on the study of analog features on other planetary bodies has been selected, further developed and tested on a relevant scenario.
This work is the result of a six-month research period at the Remote Sensing Laboratory (RSLab) of the University of Trento, from October 2018 to April 2019.

The thesis is divided into 8 chapters:

- Chapter 1: Description of Jupiter's icy moons environment, geophysical models and importance of their investigation in the context of the search for habitable spots in the Solar System.
- Chapter 2: Description of radar sounding principles and state-of-the-art on radargram simulation and interpretation.
- Chapter 3: Overview and motivation of the proposed methodology in relation to the limits of state-of-the-art on radargram simulation and interpretation.
- Chapter 4: Description of the adopted assumptions, the target modelling methodology and the correction steps necessary to obtain the simulated data.
- Chapter 5: Description of the criteria for the interpretation of the simulated data, in terms of hypotheses discrimination and subsurface interface detection.
- Chapter 6: Application of the proposed methodology to a relevant Ganymede feature.
- Chapter 7: Presentation of results
- Chapter 8: Conclusions

Chapter 1

Jupiter’s icy moons

Jupiter is the largest planet in the Solar System and the one with the largest number of orbiting satellites. Due to the extreme complexity and variety of Jupiter and its moons, it is considered one of the most important targets for space exploration and for the goal to understand the origin and evolution of our planetary system.

While Jupiter’s observations date back to ancient Babylonian and Chinese civilizations, it was not until 1610 that the existence of its moons was discovered by Galileo Galilei. Besides being one of the great milestones in the history of astronomy, the first Jupiter’s moons observation had a groundbreaking cultural and philosophical impact, providing a strong evidence against the concept of a geocentric structure of the universe.

The exploration of Jupiter and its moons began in 1973 with the first flyby by Pioneer 10 and received a consistent boost with the Voyager flyby in 1979, which showed evidence of geological activity on the Galilean satellites. The first spacecraft entering into orbit around Jupiter in 1995 was Galileo which, despite a partial failure of its telecommunication subsystem, was able to send back to Earth a large volume of data acquired during the Jupiter orbit and the numerous flybys of its moons. This mission was particularly important because it showed evidence of the possible existence of liquid water beneath the surface of Jupiter’s icy moons Europa, Ganymede and Callisto.

An outstanding peculiarity of Io, Europa and Ganymede (three of the Galilean moons together with Callisto) is the direct connection between their relative orbital motion and their geological structure and activity. In fact, their particularly stable orbital configuration (called Laplace resonance) implies the exertion of reciprocal forces that maintain their orbital eccentricity. The combination of orbital eccentricity and of Jupiter's massive gravitational field induces strong tidal dissipations within the planets and thus provides them with a significant source of energy, which could be the cause of the putative water reservoirs underneath the icy moons surface. An overview of the main characteristics of the Galilean Satellites is provided by Showman and Malhotra (1999).

The next sections of this chapter are dedicated to the description of the main characteristics of the icy moons, to the implications of the possible existence of liquid water in terms of habitability and to the description of RIME (Radar fo Icy Moon Exploration), the radar sounding instrument that has been investigated in this thesis work.

1.1 Ganymede

Ganymede is the largest satellite in the Solar System. The images acquired by Voyager and Galileo show that about 40% of its surface is covered by a heavily cratered dark terrain, while the remaining part appears as bright terrain with a higher tectonic activity and a lower crater density (Figure 2). Dark terrain is presumed to consist of a bright ice surface covered by a thin regolith layer, for the formation of which sublimation seems to play a major role. Conversely, bright terrain presents smooth surfaces with higher albedo and crossed by tectonic features like furrows, ridges and troughs. As a result of the constant rupturing of the surface due to impacts and tidal stress, some degree of porosity is expected in the shallow subsurface. Moreover, impacts and cryovolcanic phenomena could have introduced contaminants like salty impurities or rocky inclusions Heggy *et al.* (2016).

A three-layer model is currently proposed in literature for the inner structure of the satellite, consisting of a 800 km thick water ice layer, an underlying silicate mantle and a central Fe or FeS core Anderson et al. (1996). The three layers are thought to be highly differentiated. See Figure 1 for a schematic representation.

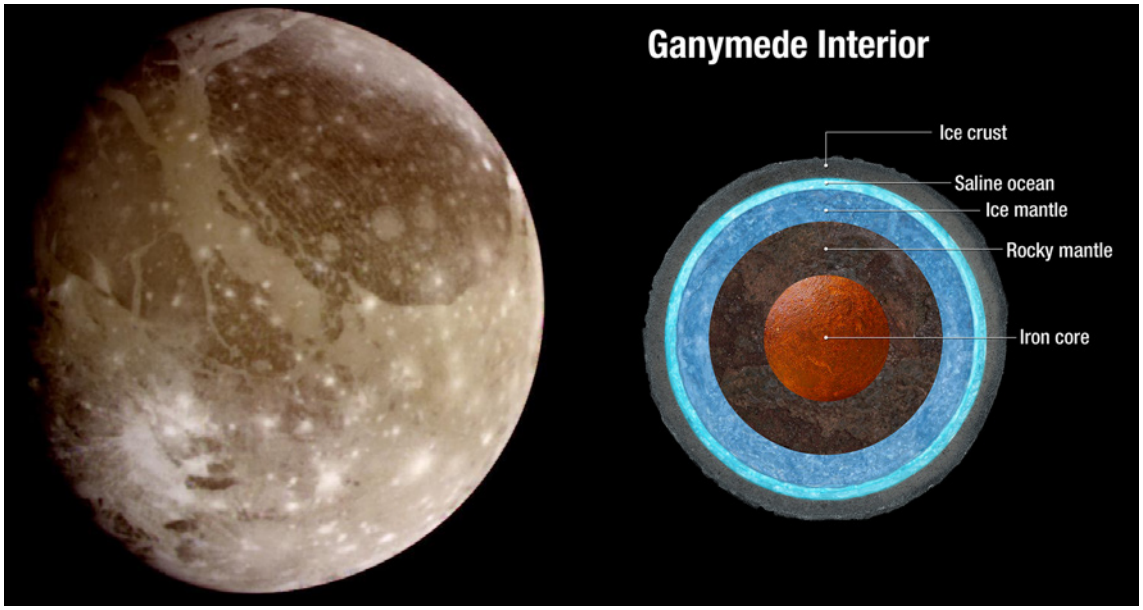

Figure 1: A picture of Ganymede's anti-Jovian hemisphere taken by Galileo and a representation of its predicted internal structure. Dark and bright terrain distinction is clearly visible in this image.

A consistent part of the analysis of the geology of planetary bodies is based on geomorphological considerations. High resolution images from Galileo allowed to identify three main formation processes of the observed features, i.e. cryovolcanism, impact ejecta fluidization and downslope movement of loose material. A thorough geological global mapping of Ganymede carried out by Patterson *et al.* (2010) has provided a more in-depth categorization of Ganymede's geomorphological features. In that work, the prevalent types of surface structures are described both for dark and bright terrain. On dark terrains, the most common types of surface geological features have been divided into three types: cratered, lineated and undivided. Similarly, bright terrain units have been divided into four main types: grooved, subdued, irregular and undivided.

Impact features appear to be some of the most important signatures on Ganymede, in that they are ubiquitous throughout its surface. They are generally subdivided into three main categories: craters, basins and palimpsests.

A considerable part of Ganymede's morphological features is supposed to be due to tectonic deformation of preexisting terrain, such as horst-and-graben faulting or domino-style tilt-block normal faulting. Although the presence of tidal forces is

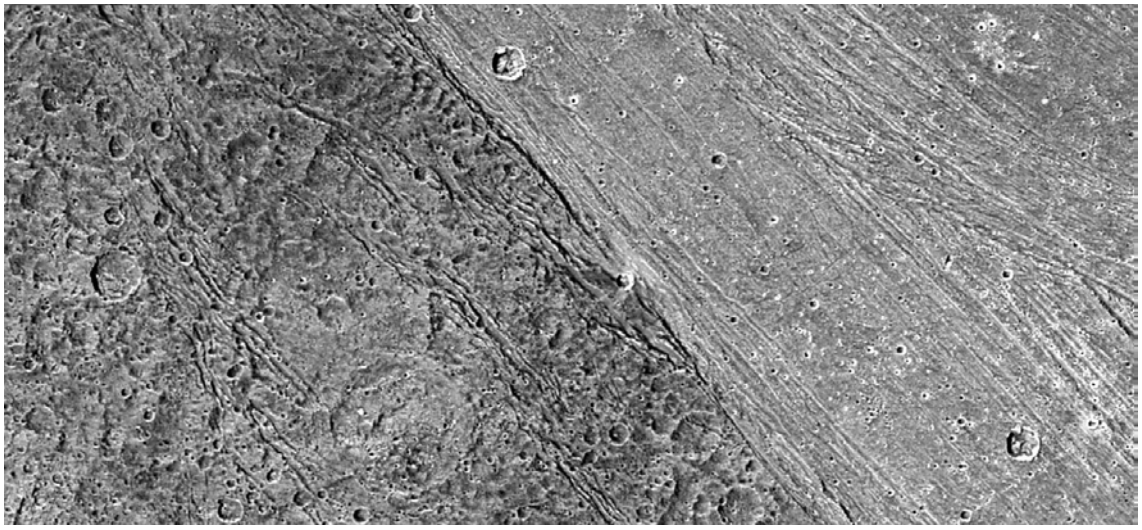

Figure 2: Ganymede's dark (left) and bright (right) terrains. The lower crater density of bright terrain due to frequent resurfacing processes is clearly visible.

undeniable for Ganymede, a better understanding of the formation dynamics of these features is fundamental to determine the role that tides could have played in Ganymede's geomorphological evolution.

Voyager and Galileo images also show small cryovolcanic flow signatures, which could hint at cryovolcanism being a secondary source of surface deformation. Nevertheless, the absence of typical cryovolcanic landforms suggests that cryovolcanism could have played a minor role in the history of Ganymede's resurfacing processes.

The analysis of surface features is a powerful tool to derive important information about the subsurface geology, considering that no direct sampling of deep subsurface material is possible with nowadays' technology. Remote sensing techniques (such as radar sounding, the object of this work) implemented in future missions to the icy moons will allow to characterize the relationship between subsurface structures and their surface expression and will help to constrain geological formation dynamics.

Ganymede is the only known moon with an intrinsic magnetic field. The presence of a subsurface water ocean has been tentatively suggested based on the detection of an induced magnetic field but, due to the complex interaction between Jupiter's and Ganymede's magnetic fields, this evidence should be supported by e.g. plasma, particles and wave observations to provide significant results. Among the technologies available today, radar sounding is expected to provide an outstanding contribution in this regard

Grasset *et al.* (2013), potentially allowing to investigate the crust structure and its interaction with the putative subsurface ocean.

1.1 Europa

Europa is the first icy moon in order of distance from Jupiter and, for this reason, the one in which tidal forces are strongest. In fact, Voyager observations show that the density of impact craters is considerably lower with respect to the other icy moons, suggesting an active geological history involving continuous resurfacing processes. From Voyager and Galileo images we can see that two main terrain types characterize the surface of this moon: smooth terrain crossed by ridges and lineae; and mottled terrain in which chaotic regions with disrupted ice blocks can be observed (see Figure 3). A comprehensive discussion of the relationship between tidal interactions and surface features is presented in Greenberg (2008).

Tidal forces seem to be the predominant factor in the evolution of Europa's smooth terrain morphology, with ridges probably resulting from tidal lithospheric compression and successive expulsion of material from the fracture. Conversely, a number of processes seem to originate chaotic terrain, such as convective activity, cryovolcanism and ice melting.

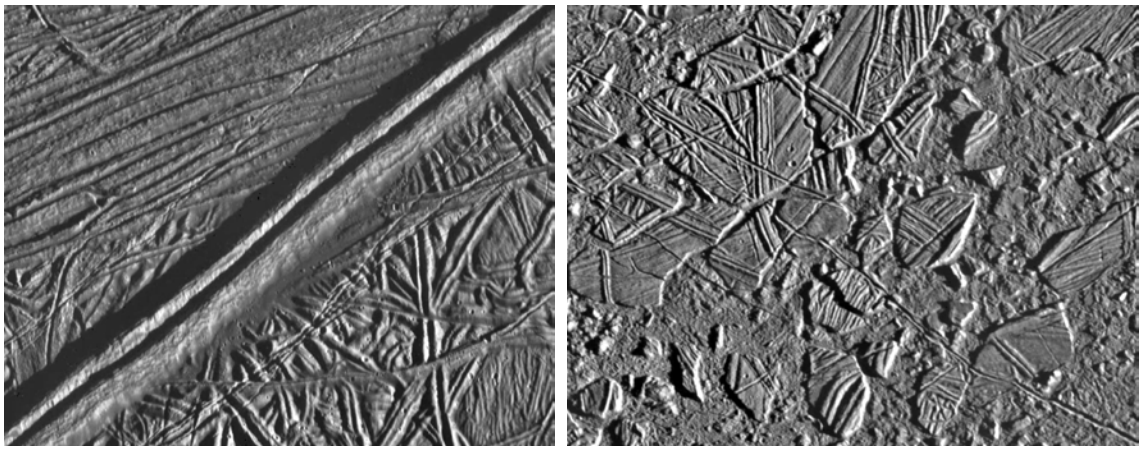

Figure 3: Europa's smooth terrain (left) with an example of a ridge and mottled terrain (right) with typical disrupted ice blocks.

Similarly to Ganymede, a three-layer model is currently proposed for Europa Anderson (1998), with an outer H_2O layer of about 80 to 200 km, an underlying silicate mantle and a Fe or FeS metallic core.

Europa's surface is the one presenting the highest content in water ice, with a spectrum that closely approximates that of pure water ice. Spectral observations carried out by NIMS (Near Infrared Mapping Spectrometer) also show non-water-ice materials, with hydrated compounds such as sulfuric acids and hydrated salts. The presence of this peculiar contaminants, together with magnetic field data acquired by Galileo, is suggested to support the hypothesis of the existence of a subsurface water ocean, with a thickness varying from several to tens of kilometers, from which those contaminants would have emerged due to surface fracturing McCord *et al.* (2001). Moreover, the high relative displacement of large crustal blocks observed in some regions would require the underlying presence of liquid water or soft ice.

Although no precise estimate of the shallow crust composition is possible at the moment, recent estimates by Heggy et al. (2017) and Aglyamov et al. (2017) suggest that radar sounding instruments could have a penetration capability of 1 to 18 km, which is compatible with the expected crust thickness. This translates into the concrete possibility of radar sounding instruments to directly detect the putative crust-ocean interface.

1.3 Callisto

Callisto is the farthest icy moon from Jupiter. Voyager images show that this satellite is considerably highly cratered (see Figure 4) with respect to the other icy moons and does not show any sign of tectonic or cryovolcanic activity. The major geomorphological processes involved are then thought to be impact cratering and thermal redistribution of materials. The main visible features on Callisto's surface are *knobs*, a result of sublimation processes acting on impact craters.

A three-layer model is proposed for the internal structure of Callisto as well, with a central iron core of up to 50% of its radius, an intermediate rock/ice mixture layer and an outer ice water layer 0 to 500 km thick. The particular morphological appearance of Callisto's craters suggests that ice is the most prominent material in its shallow crust,

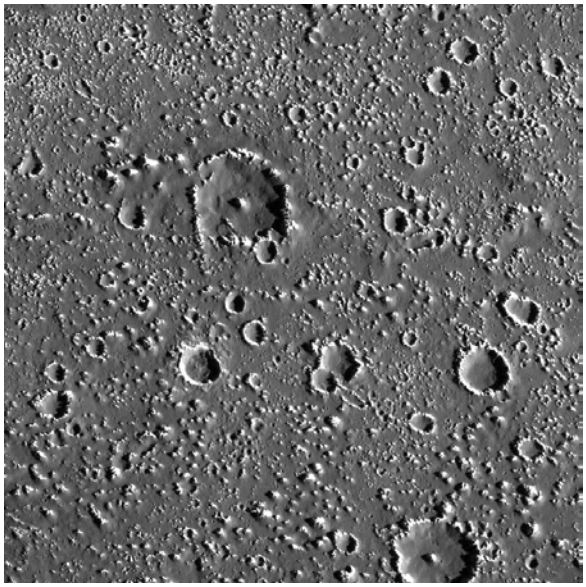

Figure 4: Image of Callisto's highly cratered terrain taken by Galileo.

corroborating the idea of an at least partially differentiated interior. Nevertheless, the investigation based on Voyager and Galileo data carried out so far has not been able to rule out either completely differentiated or undifferentiated models.

Although magnetic field data from Galileo are compatible with the existence of a liquid water layer beneath the surface of Callisto, its presence would require either different rheological properties than expected or the existence of an anti-freeze contaminant in the ocean. In any case, a liquid water layer is scarcely compatible with a partially differentiated model, making Callisto the least favourable target for the search of a subsurface ocean among Jupiter's icy moons.

1.4 Habitability

The search for habitable environments outside the Earth has always been one of the main ambitions of space exploration. In the NASA Astrobiology Roadmap (Des Marais, 2003), one of the main goals in this regard is to *"Determine any past or present habitable environments, prebiotic chemistry, and signs of life elsewhere in our Solar System. Determine the history of any environments having liquid water, chemical ingredients, and energy sources that might have sustained living systems. Explore crustal materials and planetary atmospheres for any evidence of past and/or present*

life". Among the several planetary bodies in which the basic requirements for habitability could be met (e.g. Mars, Titan, Enceladus), Jupiter's icy moons represent a promising target due to the possibility that large quantities of liquid water reservoirs exist underneath the surface. In order to refine our understanding of potential habitable environments in these planetary bodies, it is necessary to develop experimental methods and technologies that allow us to carry out both remote and *in situ* scientific investigation.

Some of the main factors determining the probability of the existence of habitable environments on planetary bodies include orbital properties, bulk composition and proper chemical ingredients. The surface of Jupiter's icy moons is an extremely harsh environment and most likely unsuitable to life, due to the extremely low temperatures and the powerful wave and particle radiations. Although the surface is the first place where one would intuitively look for present or past signs of life, potential water basins or oceans beneath the surface of Ganymede and the presence of salty compounds like sulfates and chlorides indicate that it could have all the main prerequisites to be habitable. Moreover, since the possibility of shallow habitable environments in this moon are scarce, it is thought that no strict planetary protection standards should be applied, reducing the technical constraints on future direct exploration missions Grasset *et al.* (2013).

Similar considerations can be made for Europa, in which an even higher probability of detectable habitable environments is envisaged. In fact, its icy crust is thought to be thinner with respect to the other icy moons (see previous sections for details). On one hand this implies a higher probability of processes linking the surface to the putative underlying ocean, increasing the potential to investigate the ocean's composition by sampling the material on the surface; on the other hand, the small crust thickness would be compatible with the state-of-the art capabilities of radar sounders and could result in the detection of the water-ice interface.

In order to increase the expected scientific return of the planned missions to the Jupiter system (in particular of those in which radar sounding investigation is involved) and their ability to identify potential habitable environments, the development of numerical models to constrain the properties of deep subsurface targets is of fundamental importance.

Jupiter Icy Moons Explorer	
Key science goals	**The emergence of habitable worlds around gas giants** Characterise Ganymede, Europa and Callisto as planetary objects and potential habitats Explore the Jupiter system as an archetype for gas giants
Payload	**Ten instruments** Laser Altimeter Radio Science Experiment Ice Penetrating Radar Visible-Infrared Hyperspectral Imaging Spectrometer Ultraviolet Imaging Spectrograph Imaging System Magnetometer Particle Package Submillimetre Wave Instrument Radio and Plasma Wave Instrument

Table 1: JUICE's main science goals and list of instruments.

1.5 JUICE

Two missions are planned for launch to the Jupiter system in the near future: NASA's Europa Clipper and ESA's JUICE (Jupiter Icy Moons Explorer). The two spacecrafts, whose launch is programmed for 2022, will carry out complementary investigations of Jupiter and its moons and will represent a great opportunity to drastically improve our understanding of their structure, composition and geological evolution.

The main goal of JUICE is the investigation of Ganymede and, to a lesser extent, Callisto. A suite of instruments have been designed in order to be able to acquire a wide variety of data and guarantee a comprehensive description of icy moons properties. JUICE's main science objectives and a list of the instruments is presented in Table 1.

Chapter 2

Radar sounding

Radar sounding is a technique that allows to remotely investigate the subsurface of a planetary body through the pulsed transmission of radio signals. The potential of this technology for glaciology was first demonstrated during an investigation of U.S. Army researcher in 1957, when the transparency of polar water ice to radio waves was observed. The first radar sounder dedicated to space exploration was ALSE (Apollo Lunar Sounder Experiment), launched as a payload of Apollo 17 mission to characterize the subsurface morphology of the Moon. Radar sounding investigation was recently extended to the exploration of Mars with MARSIS (Mars Advanced Radar for Subsurface and Ionosphere Sounding) and SHARAD (SHAllow RADar), launched respectively in 2003 and 2005. The former has very recently provided very strong evidence of the presence of a subglacial water lake on the southern hemisphere of Mars Orosei *et al.* (2018).

Radar sounders have been used fo Earth investigation as well and has recently allowed to detect an ancient impact crater beneath Hiawatha Glacier in northwest Greenland Kjær *et al.* (2018). A mission concept for a radar sounder dedicated to the observation of both icy and desert areas on the Earth has been recently approved by the Italian Space

Agency (ASI). The mission is named STRATUS (SaTellite Radar sounder for eArTh sUb-surface Sensing) and is coordinated by the RSLab.

Two radar sounders are planned to be launched soon to the Jupiter system: RIME and REASON. RIME, which is expected to provide groundbreaking information on Ganymede's geology, is the main object of investigation of the present work.

In this chapter the basic principles of this technology will be presented, including a rudimentary description of the necessary processing steps, the most common methods for radargram simulations and some example of the state-of-the-art in radargram interpretation. Finally, a brief description of RIME and its main parameters will be given.

2.1 Principles of radar sounding

Radar systems are based on the transmission of electromagnetic signals in order to detect the presence of targets in the field of view of the instrument, by recording the reflected electromagnetic power.

A typical radar sounding configuration is shown in Figure 5.

Let us first assume that the wave is propagating in vacuum. Considering that electromagnetic waves propagation has a finite velocity, it is possible to measure the distance r of the reflecting target from the emitting antenna by means of the equation:

$$r = \frac{c\Delta t}{2} \tag{1}$$

where c is the speed of light in vacuum and Δt is the measured delay time between transmission and recording of the reflected signal.

In case the wave is not propagating through vacuum, which is the typical scenario of ice penetrating radar investigations, the speed of propagation of the wave through the medium will be lower and can be calculated by:

$$v = \frac{c}{\sqrt{\varepsilon_r \mu_r}} \tag{2}$$

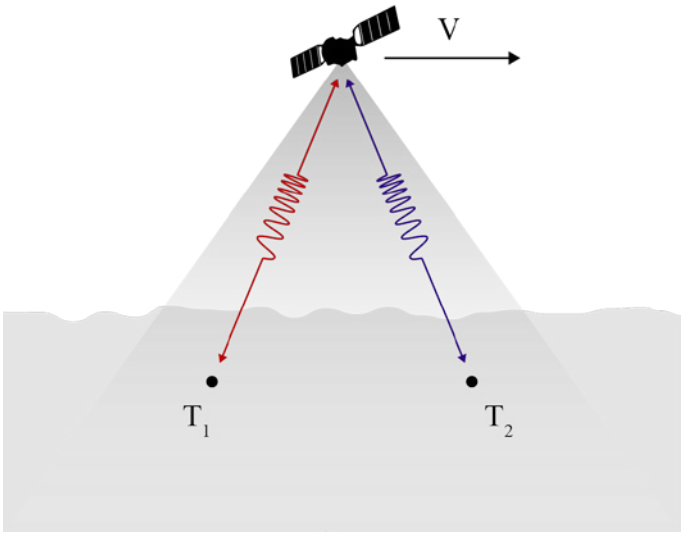

Figure 5: A representation of a typical radar sounding acquisition configuration.
T_1 and T_2 refer respectively to targets lying behind or ahead of the spacecraft with respect to its motion. The color of the echo return represents respectively negative doppler shift (red) and positive doppler shift (blue) due to the relative motion between the spacecraft and the targets.

where ε_r and μ_r are respectively the dielectric permittivity and magnetic permeability of the medium.

Dielectric permittivity is one of the main parameters affecting the propagation of radio waves through materials. In fact, signal reflections happens when the transmitted wave meets a ragion in space in which a dielectric contrast is present, such as the interface between two materials characterized by different thermal or compositional properties. The reflection coefficient of a dielectric interface can be calculated through:

$$R = \left| \frac{\sqrt{\varepsilon_1} - \sqrt{\varepsilon_2}}{\sqrt{\varepsilon_1} + \sqrt{\varepsilon_2}} \right|^2 \tag{3}$$

where ε_1 and ε_2 are respectively the dielectric permittivities of the two adjacent materials.

While travelling through the medium, the electromagnetic wave propagation is subject to additional losses, such as geometrical spreading losses, scattering and surface reflections losses.

Once all these effects are taken into account, the reflected power received by the antenna can be computed by the use of the radar equation:

$$P_r = \frac{P_t G^2 \lambda^2 \Gamma}{(4\pi)(2H)^4} \tag{4}$$

where Pt is the transmitted power, G is the antenna gain, lambda is the central wavelength, H is the distance between the spacecraft and the target and **Γ** is the wave propagation factor, which depends on the distribution of dielectric properties above the target.

In order to be able to relate the recorded reflection to the transmitted signal, a pulsed transmission is required. This means that electromagnetic pulses with a duration τ are emitted at a precise frequency PRF (Pulse Repetition Frequency). In this way, each echo return is associated with a specific transmitted pulse so that the correct time delay and distance can be computed.

The maximum space interval that the instrument can investigate without ambiguities is related to the distance travelled by the signal between one pulse and the next and can be expressed by:

$$R_{\max} = \frac{c \cdot PRI}{2} = \frac{c}{2 \cdot PRF} \tag{5}$$

where PRI=1/PRF is the Pulse Repetition Interval.

The range resolution of the instrument (i.e. the resolution in the transmitted signal direction, usually nadir) is directly related to τ: in fact, two targets cannot be resolved if their distance is less than the space travelled by the wave in the time τ. Range resolution can then be computed by:

$$\delta r = \frac{v\tau}{2} \tag{6}$$

Nevertheless, since the average transmitted power is proportional to τ and to the pulse peak power, an increase in resolution can only be obtained either at the expense of a reduction in transmitted power or of an increase in peak power, the first translating into

worst detection capabilities (SNR) and the second into heavier instrumental requirements. The transmission of chirp signals is a widespread way to improve radar capabilities in this regard, although it requires further processing steps which will be briefly illustrated in Section 2.3.

The transmitted pulse energy is emitted in form of a narrow beam through a radio antenna. Most of the energy is is concentrated in the main lobe, whose beamwidth can be expressed in first approximation as a function of transmitted wavelength λ and antenna length L_a by:

$$\theta = \frac{\lambda}{L_a} \tag{7}$$

It is important to notice that, in a simple radar ranging configuration, two targets at the same distance from the transmitter cannot be distinguished if they are under the radar beam at the same time (like the two targets shown in Figure 5). The resolution in the direction of flight, called *azimuth direction*, would then be limited to the antenna footprint on the ground, which typically translates into tens of km in case of satellite acquisitions. A drastic increase in azimuth resolution can be obtained by taking advantage of the relative motion of the spacecraft and the target, which induces a Doppler shift of the reflected signal recorded by the instrument with respect to the transmitted signal.

The induced doppler shift can be quantitatively expressed by:

$$f_d = \frac{2v_{rel}}{\lambda} \tag{8}$$

where v_{rel} is the relative velocity between spacecraft and target.

For each transmitted pulse, a unique combination of delay time and doppler shift can then be assigned to each reflecting target position. From a theoretical point of view, this means that we are able to define a transformation between the observable coordinates (i.e. Δt and f_d) and the spatial coordinates (i.e. depth and azimuth position). This allows to produce a 2-D image of the investigated ground portion, called radargram.

From a practical point of view, the increase in azimuth resolution is obtained by processing all the backscattered radar echoes collected from a particular target while it remains inside the transmitted beam. The maximum achievable resolution is:

$$\delta_x = \frac{L_a}{2} \tag{9}$$

It can be shown that this is the resolution that would be achieved if the physical antenna length equalled the distance travelled by the spacecraft while illuminating the target. Since we are virtually increasing the length of the antenna, this distance is called *synthetic aperture length* and the instruments that make use of this technique are generically called Synthetic Aperture Radars (SAR).

A basic overview of the processing steps necessary to pass from the raw recorded data to the final imaged product will be given in Section 2.3.

2.2 Radargrams

Radargrams represent the final product of a radar sounding acquisition, after range and doppler focusing are carried out (see next section for details).

The vertical dimension of a radargram represents the time delay between the signal transmission and the recording of the reflected signal (fast time, t_f); each column of the radargram is called *frame*, or *range line*. The horizontal dimension represents the time at which the recorded reflection has been transmitted (slow time, t_s); . The pixel intensity represents the intensity of the recorded signal. Since no absolute calibration of the instrument can be usually carried out, the intensity is typically normalized with respect to some predefined reference level and no information about the absolute reflected power is provided.

In order to relate the radargram appearance to the actual geological structure, further considerations and corrections must be made. The horizontal dimension can be easily related to the azimuth position x of the spacecraft, considering that $x = v_s t_s$ where v_s is the spacecraft velocity. The vertical dimension can be linked to the depth of the reflecting target through Eq. 1; since the dielectric permittivity is not constant throughout the investigated feature and is usually unknown, the passage from fast time

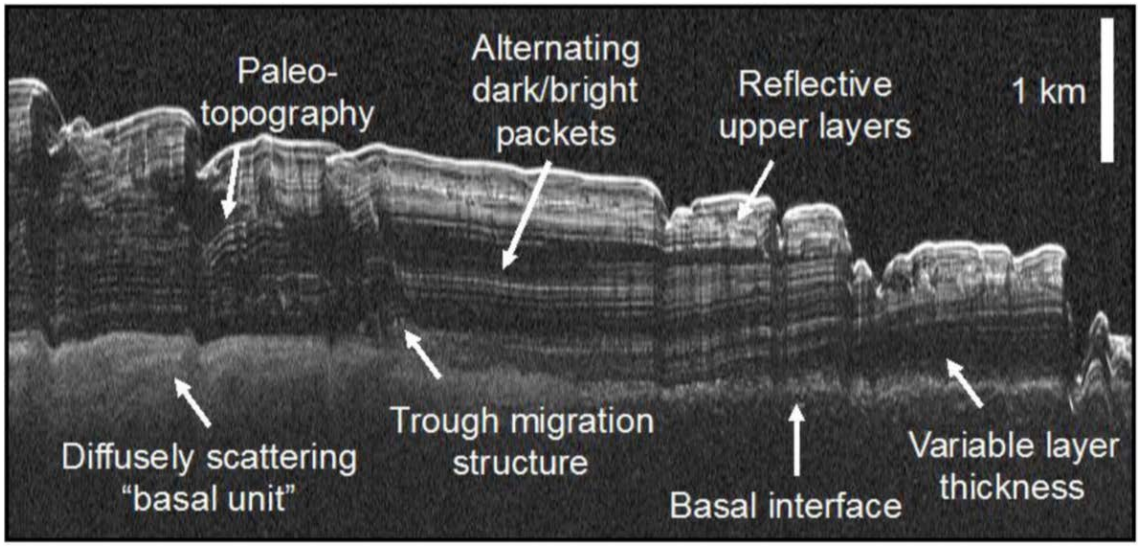

Figure 6: A radargram example, in which a number of possible features is highlighted. The vertical unit of measurement is km, indicating that the time-depth transformation has been already carried out. (Bruzzone *et al*., 2013)

domain to depth domain can only be carried out after thoughtful assumptions about the geoelectrical properties of the involved materials.

A radargram acquired by SHARAD is shown in Figure 6, in which several distinct geological structures are shown as an example of the features that can be extracted from this kind of product. The outstanding resolution obtained by range and doppler focusing can be visually appreciated.

When observing a radargram it must be taken into account that part of the reflected power comes from the across track direction (i.e. off-nadir), as the beamwidth of the transmitted wave in that direction is not null. This component of the reflected power, named clutter, cannot be directly canceled and could give rise to artifacts in form of characteristic hyperbolic shapes or image blurring. Some examples of clutter mitigation techniques will be given in Section 2.5.

2.3 Focusing

As anticipated in the previous sections, radar sounders are usually based on the transmission of chirps towards the nadir direction. A chirp is a signal in which the

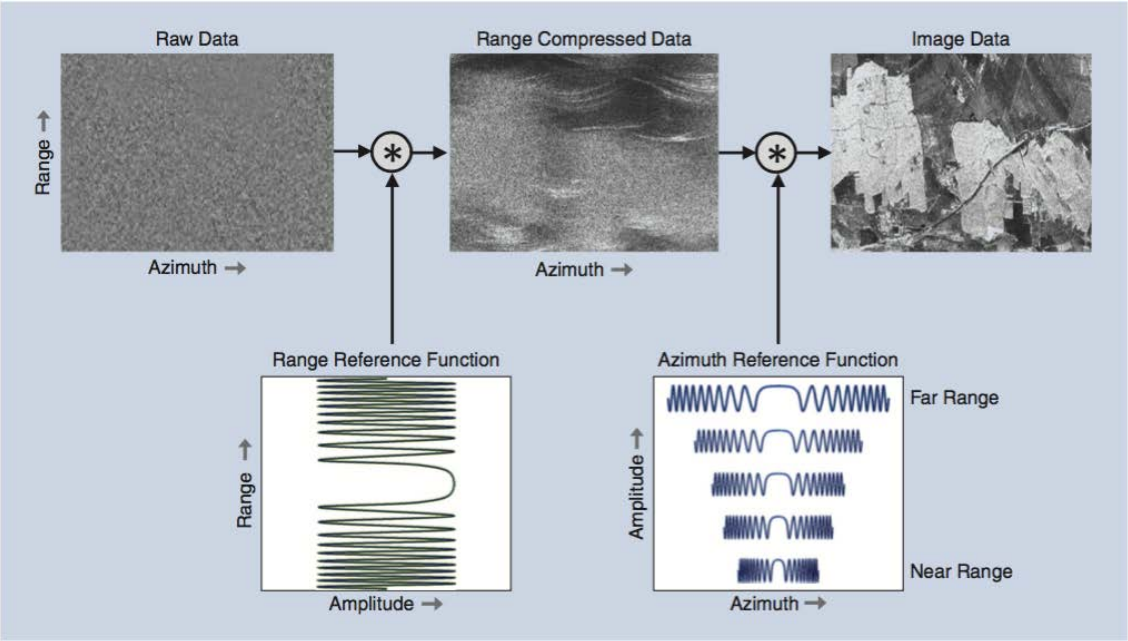

Figure 7: Diagram illustrating the mathematical operations required to focus raw radar sounder data (moreira2013). This diagram refers specifically to the focusing of side-looking radar data, but the same principles apply to radar sounding.

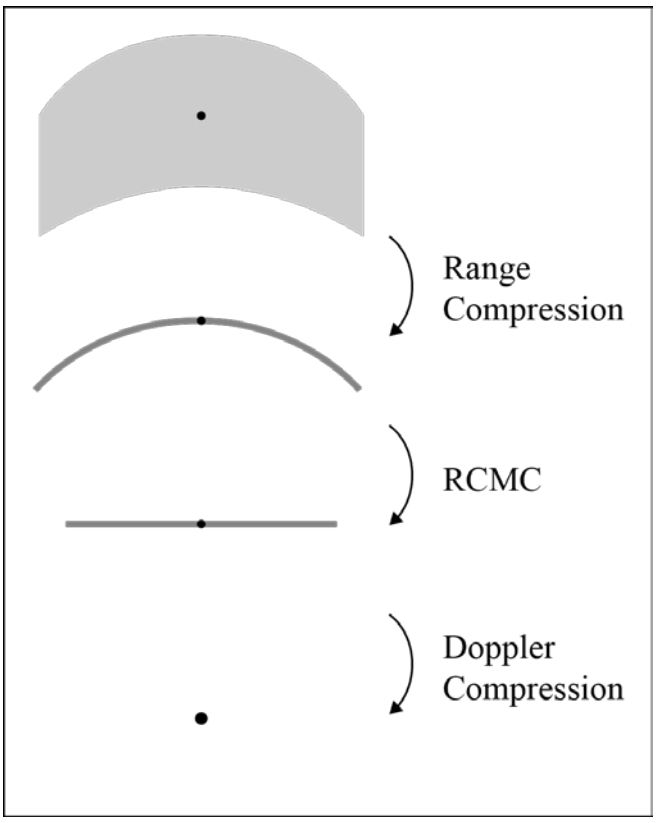

Figure 8: A schematic representation of the focusing for a single point target. The signature is originally spread both in azimuth and range directions and is successively focus by means of Range Compression, Range Cell Migration Correction (RCMC) and Doppler Compression.

frequency is monotonically modulated (usually linearly modulated, for radar sounding applications) and can be described by its central frequency f_c, bandwidth B, duration τ and amplitude A.

The processing steps necessary to properly focus the acquired scene are schematically shown in Figure 7 and Figure 8 and will be briefly explained in this section.

Let us first assume that there is one single point target in the investigated scene below the spacecraft. The echo return of the point target will have a duration comparable with τ and its signature will appear vertically spread on the radargram. Moreover, we will have an echo return for each chirp transmission (i.e. radargram column) in which the target is illuminated and the signature will then be spread in the azimuth direction as well. If no further processing is applied, the range resolution would then equal the resolution obtained by Eq. 6, while the azimuth resolution would equal the synthetic aperture length.

In order to increase the range resolution, each range line can be transformed by performing a convolution between the actual recorded range line (i.e. radargram column) and the transmitted chirp waveform (Range Compression). In order to reduce the computational load of the operation, this is practically obtained by multiplying each range line in the frequency domain by the complex conjugate of the spectrum of the transmitted signal. In this way, the originally spread signature is compressed and the distance between the target and the spacecraft (i.e. the vertical position of the target on the radargram) can be computed for each radargram column.

The achievable range resolution is then enhanced and can be expressed by:

$$\delta_r = \frac{c}{2B} \tag{10}$$

The distance of the target from the spacecraft varies during the synthetic aperture time according to a hyperbolic function:

$$r(t) = \sqrt{r_0^2 + (Vt)^2} \tag{11}$$

where r_0 is the minimum distance and V is the spacecraft velocity . The range position of the target will then be different in each column and its signature will assume the

shape of a hyperbola. This shape can be seen in radargrams obtained through technologies that cannot take advantage of the doppler shift caused by the rapid motion of the instrument, like Ground Penetrating Radar (GPR). This phenomenon is named Range Cell Migration (RCM) and must be compensated in order to cancel the coupling between range and azimuth dimensions (Range Cell Migration Correction, RCMC).
Once RCM has been properly corrected, the target signature can be compressed in the azimuth (horizontal) direction.

It can be shown that the doppler shift induced by the spacecraft motion can be expressed by:

$$f_d = -\frac{2V^2}{\lambda r_0} t \tag{12}$$

This means that the signal is linearly modulated in the slow time domain. In other words, the fast time modulation of the transmitted chirp obtained by means of electronic circuits is reproduced in the slow time domain by the very motion of the spacecraft. We can then perform azimuth (or doppler) compression following the same basic reasoning, which is by multiplying each azimuth line (i.e. radargram row) in the frequency domain by its reference function, which is the complex conjugate of the response expected from a point target on the ground.
Assuming a linear nature of wave propagation, the same methodology can be applied to a scene in which multiple reflecting targets are present, by virtue of the superposition principle.

Although several computational techniques have been devised to perform SAR focusing, all of them conceptually follow the process described above. The three most common focusing algorithm are Omega-K (ωKA), range Doppler (RDA) and Chirps Scaling (CSA). The main differences between the algorithms lie in the domain in which computations are carried out and in the specific way RCM is dealt with. For example, in CSA focusing is obtained by means of successive FFT (Fast Fourier Transform), IFFT (Inverse-FFT) and phase functions multiplications, while in ωKA data are simultaneously processed in the two-dimensional frequency (wavenumber) domain. A

number of exhaustive descriptions of these algorithms can be found in literature and is outside the scope of this work.

The basic focusing concept described above can be both applied to radar sounding and side looking radar, a different radar technique aimed at imaging the surface of planetary bodies instead of sounding their depth. Nevertheless, the final image formation process is completely different, due to the different acquisition geometries.

Moreover, the described method completely neglects the phenomenon of refraction between dielectric interfaces, an assumption which holds in case of free-space propagation (like in side looking radars) but that should be removed for radar sounding in order to increase the focusing performance. A dissertation about the influence of refraction on radar sounder data focusing can be found for example in Legarsky *et al.* (2001).

2.4 Simulation

The focusing process described in the previous chapters has been extensively used to obtain the final radargrams products from data acquired on Mars and the Moon. Another consistent part of the computer processing needed for radar sounding applications is the prediction of the instrument's performance during the design phase. For this purpose, the ability to simulate radargrams in a reliable way is of fundamental importance.

Finite Difference Time Domain (FDTD) is one of the numerical techniques currently used to simulated radar sounding data. This technique is based on the complete solution of the Maxwell's equation. In particular, it allows to solve the Maxwell's equations in time domain, providing a broadband output for a single execution of the program. FDTD is a 3D simulation technique that provides a good flexibility in modelling the target geometry, the dielectric properties of the material and the radar parameters.

In this method, both time and space discretization is required. In particular, space is discretized into elementary cells, called Yee cells, named after Yee who first introduced this method. Consequently, time is segmented into steps, called timesteps. The dimension of the cells are assumed to be small compared to the smallest wavelength involved in the simulation, i.e. the one associated to the highest frequency and highest

dielectric permittivity. In turn, time steps are comparable to the time a wave needs to travel across a cell. Let us consider that wavelengths are usually in the order of tens of meters, the investigated volume is typically in the order of cubic kilometers, the simulation time requires the signal to travel the entire depth and return to the sensor and that for each time step the Maxwell's equation need to be solved: it can be easily realized that the computational load of this methodology is huge, making the use of computer clusters unavoidable. Moreover, numerous and strong assumptions concerning the composition and structure of the investigated features are required, limiting the application of this technique to relatively simple targets. Finally, since taking into account the relative motion of the instrument and the investigated target would require even more computational capabilities, the azimuth focusing steps is not usually carried out.

Despite the difficulties related to this simulation technique, FDTD has been successfully used to simulate radar sounding data both for Mars (Heggy *et al.,* 2003) and Ganymede (Heggy et al., 2017; Sbalchiero, 2018). An example of simulated radargram can be seen in Figure 9a.

Another common approach to the simulation of radargrams are ray-tracing techniques. Ray-tracing simulators are usually based on Snell's law of refraction and on the assumption of plane wave propagation. Both coherent and incoherent methods exist, but their use is commonly limited to the simulation of surface clutter.

A new multi-layer coherent simulator has been recently proposed by Gerekos *et al.* (2018). This method is expected to provide good simulation capabilities, allowing to include an arbitrary number of subsurface layers by segmenting them into several facets, whose phase contribution is computed by linear approximation. This method is based on Huygen's principle, which states that the electromagnetic field at any point inside a control volume can be determined knowing the tangential fields on its surface. This technique seems to provide simulations that are in good agreement with real data and to guarantee a considerably lower computational load with respect to techniques based on the solution of the Maxwell's equations, such as FDTD. Nevertheless, some fundamental diffraction effects cannot be taken into account due to the plane wave approximation; moreover, surface roughness is difficult to model at small scales with this method, hindering its capability to simulate diffuse responses.

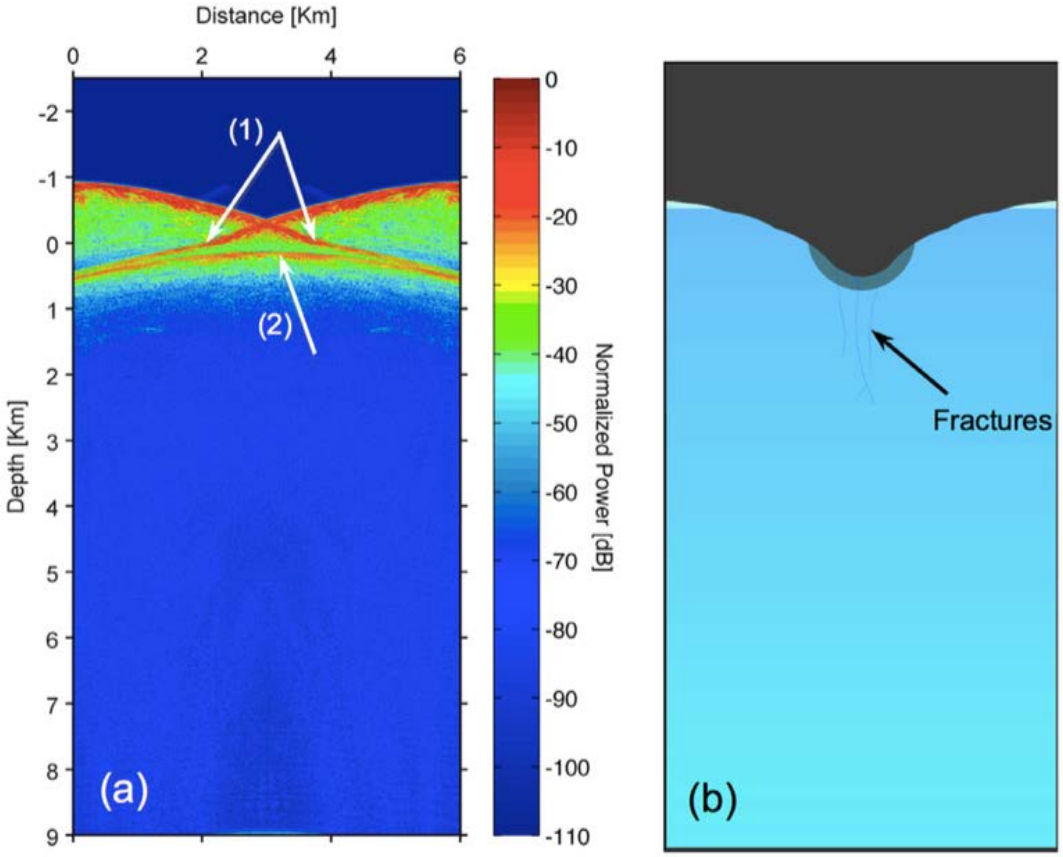

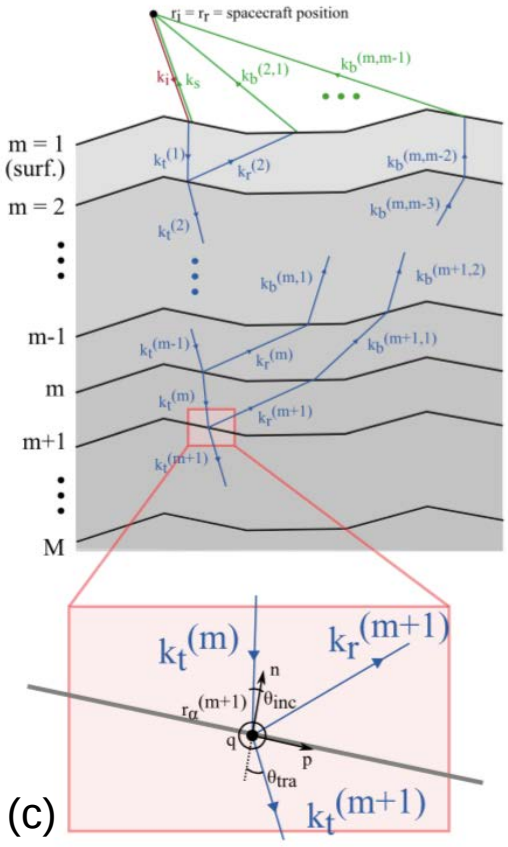

Figure 9: a) An example of a radargram resulting from FDTD simulation: the red curving signatures are due to impossibility of doppler focusing; b) the relative geological model.(Heggy *et al.*, 2017)
c) Representation of the multi-layer ray-tracing simulation technique proposed by Gerekos *et al.* (2018).

The simulation methodology followed in this work allows to cope with part of the problematics relative both to FDTD and ray-tracing approaches and is expected to be complementary to these techniques in the scope of icy moons investigation.

2.5 Interpretation

So far the interpretation of radar sounding data has extensively relied on human analysis. Although the ability of planetary scientists to extract useful information from radar sounding data remains of fundamental importance, the development of automatic interpretation algorithms represents an outstanding possibility to take advantage of the huge amount of data provided by radar sounding missions and thus maximize their scientific return.

Although automatic interpretation algorithms have not been extensively treated in literature, several approaches and techniques have been proposed in the last decade. Ferro and Bruzzone (2011) have devised a method to detect the deepest scattering area by the identification of an adequate model that best fits the radargram's statistical properties. Further work on the detection and precise location of subsurface linear features and layer boundaries has been carried out by Ferro *et al.* (2013) and Carrer and Bruzzone (2016). Finally, an automatic subglacial lake detection approach, based on successive feature extraction and automatic classification, can be found in Ilisei *et al.* (2019).

One of the greatest problems in radargram interpretation is the phenomenon of clutter, which is due to the cross-track surface returns that arise from surface topography farther away from the first-return point and therefore have a longer time delay. Due to this increased delay, the cross-track surface returns appear to originate from beneath the surface when viewed as a radargram. A common method to identify radargram features that are specifically due to clutter is based on the comparison between the actual radargram and a simulated "cluttergram", which is obtained computing all the signal returns that arise from surface features (see e.g. Choudhary *et al.*, 2016). Ferro *et al.* (2013) have proposed a similar approach, including the possibility to perform automatic interpretation of the resulting simulations through the coregistration between the radargram and the relative cluttergram and the successive automatic extraction of

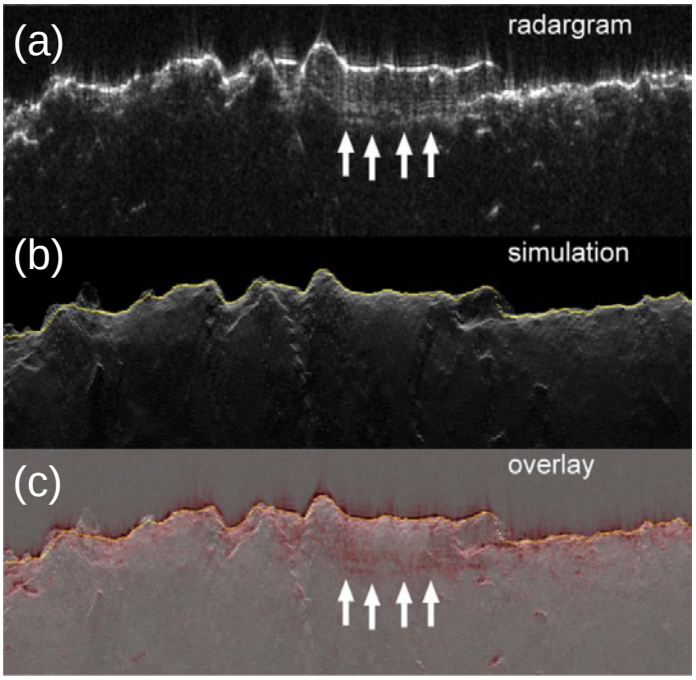

Figure 10: Representation of a typical clutter analysis. Original radargram (a) and simulated "cluttergram" (b) are superimposed (c) in order to discriminate between actual subsurface signatures and clutter artifacts. (Nunes *et al.*, 2011)

surface clutter returns from the coregistered radargrams. An example of the application of this approach is showed in Figure 10.

Most the of the techniques presented so far focus on the geostructural properties of the investigated target; the automatic interpretation of radargrams in terms of compositional, geoelectrical and thermal properties has not been sufficiently dealt with in literature. For this reason, one of the aims of this work is to propose an interpretation methodology that could support and complement the available techniques.

2.6 RIME

Among the investigation techniques implemented on the planned missions to the Jupiter system, radar sounding is the only one that will allow to directly observe and image the geological structure of the satellites down to several kilometers underneath the surface.

Main Instrument parameters	Parameter values
Transmitted central frequency (MHz)	9
Antenna type	Dipole
Optimal antenna length (m)	16 m
Peak radiated power (W)	10
Stand-by power with cont. (W)	13.3
Avg. power during sounding with cont. (W)	25.1
Penetration depth (km)	As deep as 9
Chirp length (μs)	50 - 100
Vertical resolution in ice (m)	30 - 90
Cross-track resolution (km)	2 - 10
Along-track resolution (km)	0.3 - 1.0
Circular Orbital Phase	
Orbit height (km)	200 - 500
Pulse repetition frequency (Hz)	200 - 400
Chirp bandwidth (MHz)	3, 1
Chirp length (μs)	50 - 100
Receiver window length (μs)	117 - 226
Data rate (kbps)	216 - 250
Flyby Phase	
Flyby distance (km)	< 1000
Pulse repetition frequency (Hz)	500
Chirp bandwidth (MHz)	3
Chirp length (μs)	100
Receiver window length (μs)	226
Data rate (kbps)	2400

Table 2: RIME's main instrumental parameters.

The radar sounder selected as payload for JUICE (see previous chapter) is RIME (Radar for Icy Moon Exploration). In the first part of the mission, RIME will be able to acquire data from all three icy moons during flyby passages; in the last part of the mission the spacecraft will enter a circular orbit around Ganymede, RIME's main target.

A series of fundamental questions about icy moons properties will be addressed by this instrument. Besides characterizing the satellites in terms of compositional, thermal and strucutral properties, RIME is expected to provide insights about the crust thickness, the existence of subsurface water reservoirs and the material exchange between the surface and the subsurface. RIME's main instrumental parameters are summarized in Table 2.

The choice of the 9 MHz central frequency is the result of a trade-off between penetration depth, SNR maximization, clutter reduction and propagation loss requirements. The instrument bandwidth can be selected between 1 and 2.8 MHz, allowing for a great flexibility in terms of resolution enhancement and data volume reduction (Bruzzone *et al.*, 2013).

Computational simulations provided by Heggy *et al.* (2017), based on the current knowledge of Ganymede's composition, has tentatively suggested a penetration depth capability ranging from 8 to 20 km. If these figures will be confirmed, the investigation of some of the most important structural features of the satellite, such as the putative brittle-ductile interface, will be possible.

Chapter 3

Thesis approach overview

In this chapter we will briefly explain the principles of the methodology adopted for this thesis work. In Section 3.1 the main differences between the methodology followed and the state of the art will be presented, in terms of expected results and advantages; moreover, the principal assumptions are explained. In following sections, the main steps necessary to go from the available data to the simulated data are presented.
Further details will be provided in the next chapters.

3.1 Analog approach

As mentioned in the previous chapter, a number of numerical methods are available to simulate the behaviour of radar sounders and to obtain products that mimic data from real instruments. These tools are of fundamental importance to predict how geological features will appear and to improve our present and future ability to interpret radar sounding data.
Most of the methods presented so far are broadly based on the numerical generation of the investigated geoelectrical model and on the successive analysis of electromagnetic waves propagation, based on theoretical and empirical equations. Their advantage

consists on the possibility to produce simulated data starting from arbitrary geoelectrical models and to have a complete control on the physics of the simulation, starting from the wave propagation dynamics. Nevertheless, this introduces three main problems: 1) since there is usually a considerable uncertainty on the investigated feature's structure and dielectric properties, strong assumptions must be made in order to generate the required geoelectrical models and only simplified configurations can be taken into account, 2) numerically propagating electromagnetic waves is usually very time consuming and requires great computational capabilities and 3) state-of-the-art wave propagation methods do not take into account the velocity of the spacecraft, meaning that no doppler focusing is possible.

In order to overcome these problems, a possible strategy is to leverage data available from better known features for which a similarity in geoelectrical and structural properties with respect to the investigated feature has been identified. This approach has been widely used in the history of comparative geology, since it allows to narrow down all the possible hypotheses and uncertainties and to focus on problems that have already been dealt with in literature.

Recently, a method has been proposed to use these geological analogs for radar sounder simulations by Thakur and Bruzzone (2019). The analog approach to simulation is based on the analysis of data collected from features (*analogs*) whose environment is characterized by properties analogous to what we expect to find on the investigated environment. This approach is generic and, as long as assumptions are clearly stated, can be applied to all sorts of scientific investigation and not only to geological research.

For the purpose of this thesis, the main criterion of similarity has been searched in the processes of formation of the investigated planetary body geology. This premise is necessary for the simulated results to be relevant with the investigated feature's actual expected scenario. A series of geological properties must then be selected so that analog features's formation processes resemble as much as possible those of the investigated feature.

Although the terrestrial planets and the icy moons have completely different composition, and therefore different mechanical properties, geomorphologically similar features have been observed in optical images of these bodies.

This can be explained by the similarity in homologous temperature of the terrestrial planets and the icy satellites. In the analogs approach, we extend this principle to assume similarity in the shallow subsurface morphology as well. Homologous temperature T_h is defined as:

$$T_h = \frac{T}{T_m} \tag{13}$$

where T is investigated material's temperature and T_m is its melting temperature.
The choice of this particular parameter represents an advantage in two main respects: planetary bodies' local temperature has a strong variability throughout the Solar System, making it difficult to identify a body in which temperatures are similar to those found on the investigated scenario, let alone to the extreme environment of Jupiter's icy moons; moreover, and even more importantly, most of the available geological data comes from rocky bodies, making it difficult to find data of analog features with similar composition. Using T_h as a selection criterion allows to cope with these two major problems and to leverage available data in a well-founded and effective way, extending the research of analog features to planetary bodies for which a significant amount of data is available.

3.2 Terminology

Throughout this work, a specific terminology is used to refer to the different components of the approach. We use the word *investigated* to refer to the elements of the scenario for which we are interested in obtaining simulated data (e.g. Ganymede in this work). We will then refer to the *investigated radar sounder* and the *investigated planetary body*. Conversely, the scenario from which we extract the starting data (e.g. Mars in this work) and all the elements characterizing it will be referred as *analog*. The general idea is then to pick a *reference analog radargram*, from which we numerically extract a *simulated investigated radargram* that represents an approximation of the *real investigated radargram*.

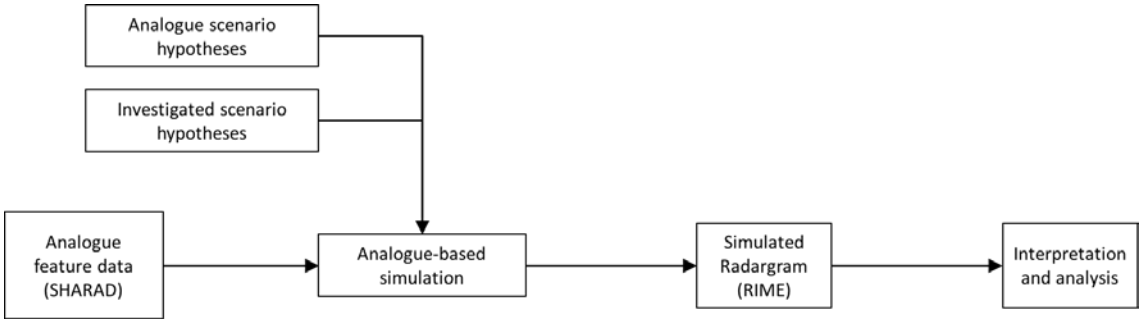

Figure 11: Schematic description of the the general methodology

3.3 Simulation methodology overview

The main object of this thesis are radargrams, bidimensional data products described in Chapter 2. Generally speaking, the method proposed in this work consists in a series of steps through which we can obtain simulated radargrams of the investigated scenario from data products available from analog features on different planetary bodies. A schematic description is shown in Figure 11.

3.3.2 Analog scenario

The first step of this method is the selection of an adequate feature on a different planetary body. A series of similarity criteria has to be identified in order to select a feature that mimics the expected structure of the investigated scenario in some crucial aspects. Such a criterion has been selected for this thesis (see previous section) but a different set of selection principles can be chosen according to the specific requirements of the investigation.

Moreover, it can be desirable that the instrument collecting the analog data share similar features with the investigated instrument, for example in terms of transmitted power, bandwidth, pulse-repetition frequency, transmitted waveform etc. Although it is not strictly necessary for these properties to be very similar between the instruments, it can help to remove any artifacts in the simulated products due to major differences in the acquisition process.

Finally, it must be assessed that the data collected by the analog instrument are sufficient and reliable. In fact, in addition to scientific data deriving from the reflected signal, a number of telemetry information is necessary for the correct focusing of the raw data and the simulation process methodology described later.

3.3.3 Analog and investigated hypotheses

As outlined in the first chapter, our knowledge of Jupiter's icy moons has greatly improved in the last decades thanks to the missions sent to the Jupiter's system. Nevertheless, most of the icy satellites' characteristics are yet to be described with sufficient confidence. Several hypotheses have been presented in literature in terms of some major geological parameters, such as the satellites' composition, temperature profile, inner structure, crust thickness and many others. Being able to determine some of these parameters with good accuracy, or at least rule out some hypotheses, would be a great step forward in the description of these planetary bodies.

The second step is then the selection of a set of characteristic and fundamental parameters through which the analog and investigated scenarios can be described. Here the word "scenario" refers to all the main factors that come into play during the acquisition phase, both from the geological and the instrumental point of view. These parameters can usually be derived by previous geological or instrumental investigation and can both be applicable to the planetary body as a whole or be specific to the particular feature chosen.

For each of these parameters, a set of two or more possible values are selected following the hypotheses made in relevant scientific or technical literature. All the possible combination of the selected hypotheses are then taken into account, in order to be able to consider the full spectrum of variability of the investigated scenario.

3.3.4 Analog-based simulation

Once the analog data are selected and available and all the combination of hypotheses are defined, it is necessary to define a set of equations through which we can correct the analog data and get the simulated data of interest. The selected equation will directly act on the value of each element of the radargram matrix, depending on the value of the

parameters corresponding to the selected hypotheses combination. This will yield a different result for each of the defined hypothesis or combination of hypotheses, corresponding to what we would expect the radargram to look like in case the scenario's parameters matched the ones listed in the selected combination. Two different data simulation methodologies have been adopted, respectively applied to pre-processed and raw data, and will be described in Chapter 4.

3.4 Database creation

The first expected result of this method is the creation of a database such that to each hypotheses combination corresponds a different simulated radargram, so that the full spectrum of variability is simulated. In this way, besides the influence of single parameters on the radargram appearance, we will be able to take into account the variations due to phenomena of parameter interdependence, including possible compensation effects. These kind of databases will potentially represent a powerful tool for successive radargram analysis, making use of the state-of-the-art automatic interpretation algorithms (see Section 2.5 for some examples) and the ones that will be developed thanks to emerging disciplines such as machine learning and artificial intelligence.

3.5 Interpretation

Besides providing the methodology and the database produced by its application to a selected Ganymede feature, some preliminary interpretation of the resulting database will be presented, in terms of the predicted ability of the radar sounder to discriminate between different hypotheses combinations and to identify subsurface interfaces.

3.5.1 Similarity

The first interpretation criterion we select is the similarity between the simulated geoelectrical models and radargrams. For this purpose, every simulated product is compared with each of the others in order to understand which parameter variations cause the strongest variation in the simulations. In this way, the sensibility of radar sounding technology to specific parameter variations can be investigated, in order to

determine target priority for future acquisitions and to help in the selection of adequate instrumental parameters for specific types of feature.

3.5.2 Detectability

The second interpretation criterion focuses on the ability of the radargram to detect subsurface structures. In fact, one of the main objectives of future icy moons exploration is the comprehensive study of their geology, which requires to relate subsurface features to their surface expression by comparing for example imaging data to the relative radar sounder acquisitions. Subsurface interfaces due to compositional and thermal discontinuities are among the most important objects of investigation of radar sounders, due to the radio reflections caused by dielectric contrast. For this purpose, the emergence of subsurface interface signatures in the simulated radargram has been investigated for each hypotheses combination by quantitatively comparing subsurface reflections respectively with surface reflections and average noise level, in order to identify the parameters that determine a higher detectability of this particular type of subsurface feature.

Chapter 4

Data simulation

In this chapter we will explain the steps necessary to pass from the analog radar sounding data to the simulated data. The aim of this thesis work is to provide a comprehensive view of the major factors affecting the parameters of radar sounding, which can be broadly divided into geoelectrical, instrumental and data processing factors. The description is then divided into two parts, corresponding to the two phases in which the work was carried out:

- In the first part of the work we focused on the analysis of geoelectrical and instrumental parameters. The simulation methodology proposed by Thakur and Bruzzone (2019) has been selected and will be briefly summarized in Section 4.1 for completeness. The method described requires to use pre-processed data (i.e. after range and doppler compression described in *chapter 2*) as original analog data, in order to minimize the influence of the focusing process on the results. However, in this approach it is not possible to understand the effects of some of the data acquisition and raw-data processing parameters (e.g. PRF, spacecraft velocity, SAR focusing etc.)
- For this reason, in the second part of the work we have proposes an approach to include the focusing process in the simulation methodology. This requires to use

unfocused raw data as a starting point, in order to understand how the focusing parameters can affect the quality of the radargram and our ability to extract useful information from it.

4.1 Pre-processed data methodology

As briefly mentioned in the previous paragraph, the first part of the work focused on the impact of instrumental and geoelectrical parameters on the radargram characteristics. In this section the selected methodology, which is the one proposed by Thakur and Bruzzone (2019) with some minor adjustments, will be described. This type of analysis requires us to eliminate as many data processing factors as possible that could have an impact on the final result. For this reason, the selected starting data are analog radargrams that have already been processed through range and doppler compression.

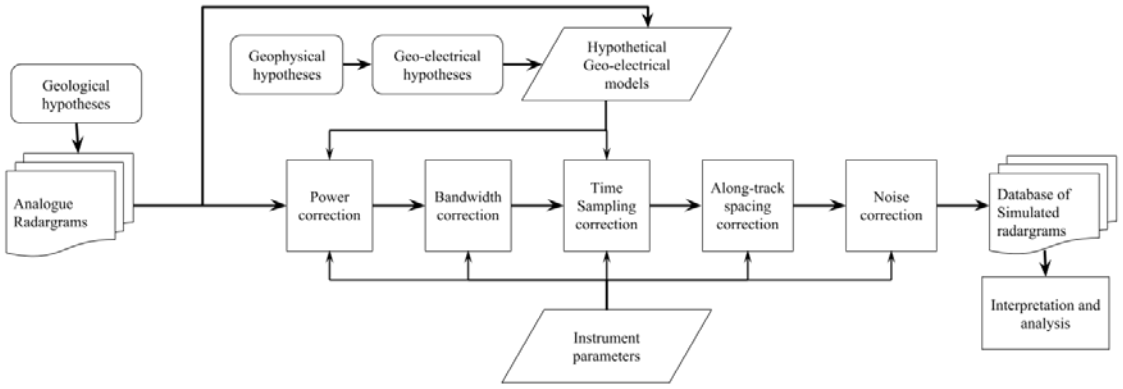

Figure 12: Schematic description of the steps relative to the pre-processed data methodology.

Assumptions

The methodology described is based on a set of assumptions related to the similarity between the analog and the investigated feature. These assumptions need to be clearly stated in order to understand in which cases the method can be applied and when, on the contrary, some further attention should be payed on the characteristics of the two features.

1) *Geometrical similarity:* The first thing we assume is that the geometry of the two features is similar, in terms of the shape of the surface and of the position of the dielectric interfaces. Although some differences are expected in this regard, geometrical similarity is supported by the similar processes of formation undergone by two planetary bodies in the presence of comparable homologous temperature.
   This assumption does not relate to the scale in geomorphology, which can be significantly different between the two features.
2) *Noise similarity:* We assume that the noise is addictive and not signal dependent both for the analog and the investigated instrument. We further assume that the noise statistical distribution is the same for both scenarios. This allows us to stochastically compare the difference in noise power levels of the two scenarios.
   Although Jupiter's electromagnetic noise is in general a major factor to take into account, for this thesis work we have only considered cosmic background as a noise source, in order to reduce the expected difference between noise distributions in the compared scenarios. This means that, for the moment, the only targets we can consider are those on the anti-Jovian side of the icy satellites.
3) *Geo-electrical models:* The method proposed requires to assume the geo-electrical properties of the analog and investigated scenarios. Since no direct measurement of these parameters is currently available, assumptions in this regard will be based on the current state-of-the-art prediction of geo-electrical properties of Jupiter's icy satellites.
4) *Surface roughness:* As mentioned in *chapter 2*, clutter is one of the main sources of uncertainty in the analysis of radargrams. Clutter mainly depends on the target's topographycal characteristics and on surface roughness, which are usually described through Digital Elevation Models (DEM). Since DEMs are not always available for Jupiter's icy moons, a direct comparison on the influence of clutter is not possible. For this reason we assume that the clutter contribution to the radargram is the same for the analog and investigated features.

Although the described assumptions are rather strict, it is important to notice that the proposed method is very flexible in handling the simulation inputs. With more data

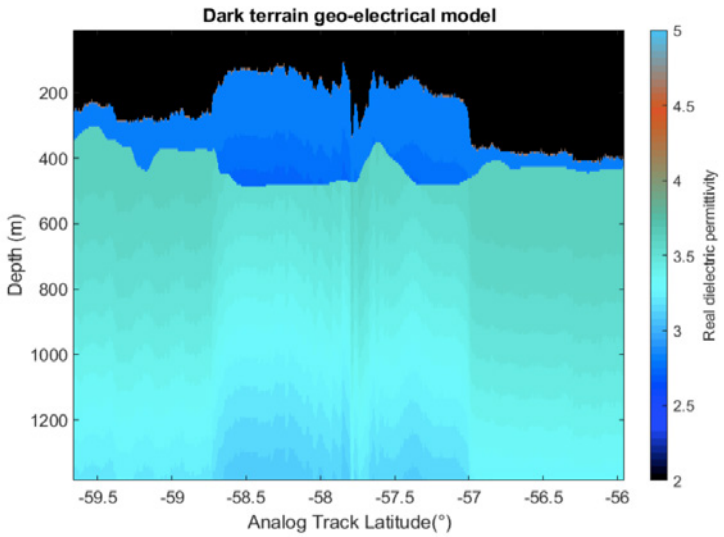

Figure 13: Example of a geoelectrical model obtained by the target modelling methodology followed in this work (Thakur and Bruzzone, 2019)

from the investigated scenario, the uncertainty introduced by these assumptions can be subsequently reduced.

Target modelling

The starting data consist of a radargram acquired on the analog target. The correction steps necessary to pass from the analog data to the simulated data require to define a geoelectrical model based on the geological shape emerging from the radargram image. This means that a particular complex dielectric permittivity needs to be assigned to each pixel of the image.

The geoelectrical modelling methodology of the investigated feature will be described in detail in Chapter 6.

For what concerns the analog feature, this phase has required to make some simplification with respect to the real expected characteristics of the analysed geological feature, since no adequate description of the subsurface composition of the selected feature on Mars has been presented in literature so far. In general, geoelectrical parameters change in a continuous way throughout a geological volume, depending on several factors like temperature, composition, porosity, impurity etc. Nevertheless, it is particularly reasonable to identify some regions in which dielectric properties are nearly homogenous, due to some expected similarity with regard to the aforementioned factors.

These similarities are feature dependent and must be assessed time by time, based on the information retrieved by state-of-the-art investigation on the characteristics of planetary bodies.

Most of the investigation carried out through radar sounding aims at the identification of geological layerings underneath the surface of rocky/icy planetary bodies. This means that we assume that some relatively homogeneous regions are divided by dielectric interfaces. These dielectric contrast are the ones that induce signal reflections, due to electromagnetic propagation properties illustrated in Chapter 2.

This means that we must identify a value for the complex dielectric permittivity for each zone comprised between two dielectric interfaces, assumed constant throughout each identified zone.

The area of the image above the surface represents the free space that the electromagnetic signal has to go through between the antenna transmission and the first surface detection. Due to the near-vacuum characteristics of the atmospheres of the planetary bodies taken into account, the dielectric permittivity of this zone is assumed to be the same as vacuum permittivity. This zone is of particular importance in order to estimate the statistical properties of noise for the investigated scenarios. Considering that no absolute calibration is usually carried out for radar sounding instruments, noise level is a major reference point in order to evaluate the actual intensity of target reflections, in terms of signal to noise ratio.

Correction steps

Once a specific dielectric permittivity value has been assigned to each region/pixel of the acquired feature, we can apply a set of corrections to the radargram in order to obtain the simulated radargrams for each hypotheses combination. The necessity of the geoelectrical modelling step described in the previous paragraph will now result clear, as the dielectric permittivity distribution is the most important parameter influencing the electromagnetic signal propagation through a medium.

1) *Signal magnitude correction:* as stated before in the text, one of the assumptions of this work is that the noise component of the recorded wave is the same for the analog and the investigated features. Nevertheless, the power reflected from dielectric interfaces and targets cannot be assumed to be the same, even assuming

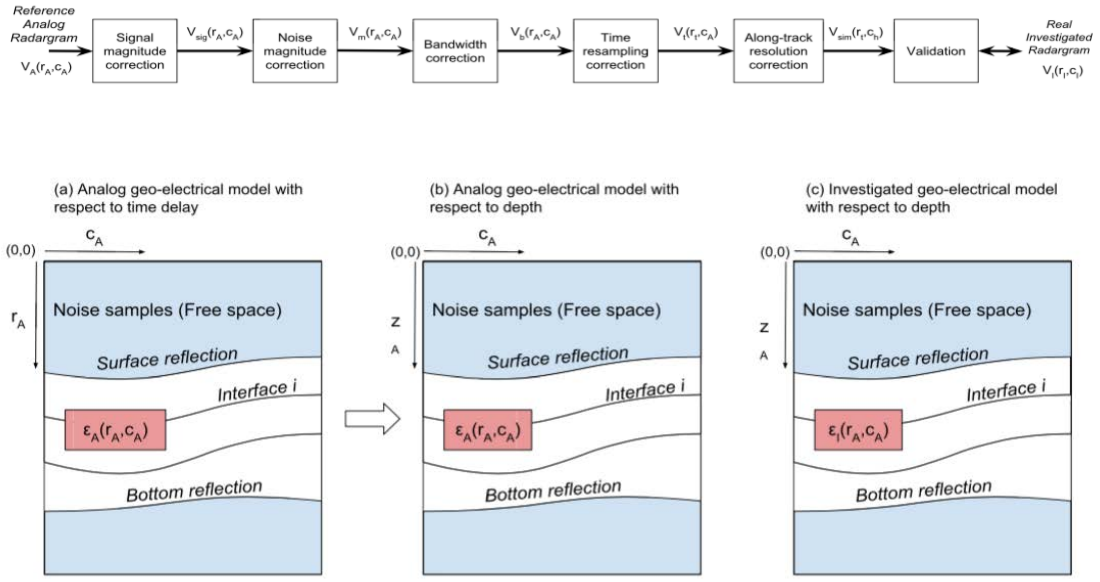

Figure 14: Above: methodology flowchart of the methodology proposed by (Thakur and Bruzzone, 2019); Noise and along-track resolution corrections have not been carried out in this work. Below: schematic description of the depth correction step.

geometrical similarity between the analog and investigated features. In fact, the amount of electromagnetic power returning back to the receiving antenna does not only depend on the target's geometrical configuration but from a combination of different factors that can be expressed through the Eq. 4 presented in Chapter 2. Although no absolute calibration is possible either for the analog and investigated acquisition, it is useful to perform a relative calibration between the analog and investigated scenario, in order to understand how the several parameters at play impact on the amount of power reflected from dielectric interfaces. It is then possible to correct the power of each radargram pixel considering the ratio $P_{r,I}/P_{r,A,}$ where the reflected power is computed through Eq. 4.

Notice that the amount of correction applied depends both on instrumental and geoelectrical hypotheses. In particular, the wave propagation factor $\boldsymbol{\Gamma}$ directly depends on the vertical distribution of dielectric permittivity above the reflecting target.

2) *Bandwidth correction:* another fundamental parameter affecting the quality of a radargram is the bandwidth of the transmitted signal. As described in Chapter 2, a

common technique used in radar instruments is the transmission of a chirp signal, instead of an impulse or a single sine wave. The main radargram feature impacted by bandwidth is range resolution, according to Eq. 10. Two possibilities can then present for us, as the bandwidth of the investigated instrument can either be smaller or greater with respect to the analog instrument bandwidth.

In the first case we need to numerically decrease the effective bandwidth of the instruments. For this purpose, we need to transform each frame of the radargram to the frequency domain and apply a low pass filter in order to obtain the required bandwidth.

The second case is more critical, as numerically increasing the bandwidth of the signal means to artificially increase the range resolution of the radargram. This in turn means to virtually increase the information content of the radar product. In fact, by increasing the signal bandwidth we are only increasing the sharpness of the image and not the information content of the subsurface region. Nevertheless, this still constitutes a valuable tool to visually understand how a radargram would appear in the investigated scenario.

3) *Depth correction:* as explained at the beginning of the paragraph, we assume that the the analog and investigated feature share a similar geometry. Nevertheless, what is actually represented in the vertical dimension of a radargram is not the real depth but the delay time between transmission and recording of the signal. This means that the apparent position of a target on the radargram does not depend on its physical position only, but also on the distribution of dielectric permittivity along the transmitted signal path. This is due to the fact that the speed of light in a medium is related to dielectric permittivity through Eq. 2.

   This means that, once a dielectric permittivity value has been assigned to each region of the acquired feature, we can relate each point target's delay time with its expected depth and vice versa, allowing to correct the position of the target in the analog radargram in order to obtain its position on the investigated radargram. An illustration of this processing step is showed in Figure 14.

4.2 Raw data methodology

Conversely to what has been done in the first part of the work, in the second part we chose to focus on the data processing step of the radargram formation process. This decision was made in order to be able to take into account all the main types of factor that come into play when performing radar sounding, i.e. geoelectrical, instrumental and data processing factors.

For this reason, geoelectrical parameters were completely taken out from the simulation methodology and only the instrumental parameters that have a direct impact on the radargram processing steps were taken into account.

The expected result of this work is to understand how some of the main parameters affecting the focusing process impact the radargram quality and our ability to obtain valuable information from it.

Assumptions

As done for the description of the first part of the work, the main assumptions made will be explained in order to clearly state in which conditions this method can be applied with sufficient confidence.

1) *Geometrical similarity:* similarly to what assumed in the first part, the geometry of the acquired featured is assumed to be similar between the analog and investigated scenario (see previous section for details).
2) *Noise similarity:* the same is valid for noise power and distribution. (see previous section for details)

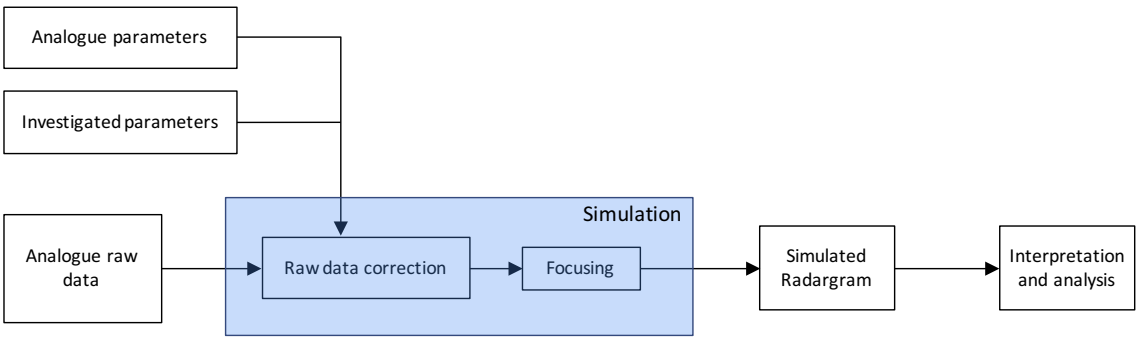

Figure 15: Schematic description of the steps relative to the raw data methodology.

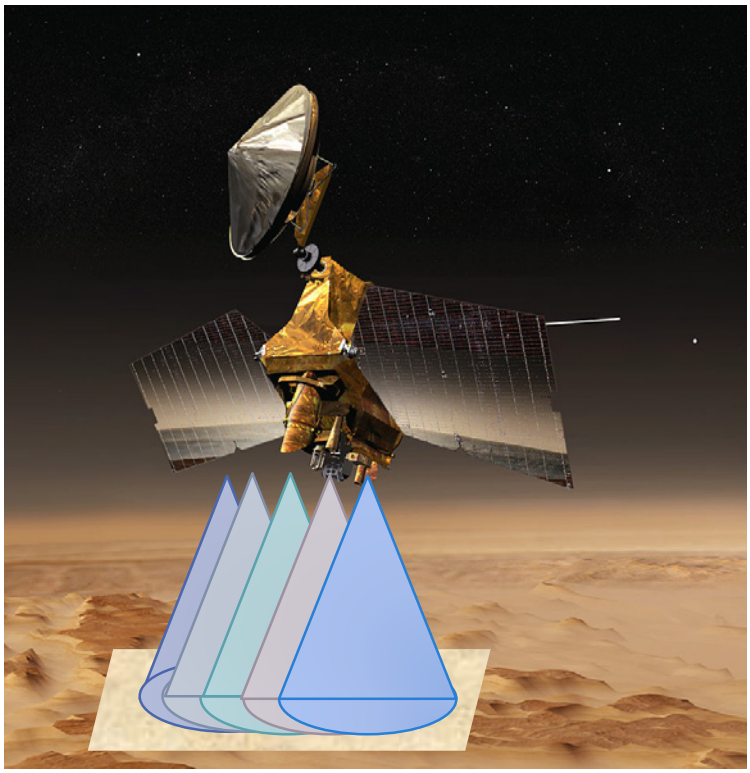

Figure 16: Schematic illustration of the acquisition phase, in which multiple signals are transmitted as the spacecraft moves along its orbit.

3) *Surface roughness:* the same is valid for noise power and distribution. (see previous section for details)

4) *Geological continuity:* we assume that the geological and geoelectrical properties vary in a continuous way throughout the investigated target and that the scales of variation of potential discontinuities are much grater than the analog radargrams resolution.

Acquisition modelling

As explained in Chapter 2, two of the main steps necessary to obtain a radargram are range and doppler focusing. Both range and doppler focusing have two fundamental properties impacting the quality of a radargram: 1) they improve resolution and 2) they increase signal to noise ratio (SNR). In the context of radar sounding, an increase in resolution mainly translates into the ability to distinguish finer structures in the

geological volume of interest, while an increase in SNR allows to identify in a clearer way the presence of geological targets and dielectric interfaces.
One of the main parameters that comes into play in order to obtain a proper doppler focusing is the spatial distance between two successive acquisitions, i.e. two successive columns of the radargram. With distance we basically mean the space that the spacecraft travels between an acquisition and the next.

This value is determined by several instrumental and orbital parameters, which in our case can be summarized into:

1) Spacecraft velocity (V): this represents the spacecraft velocity component parallel to the ground.
2) Pulse Repetition Frequency (PRF): the frequency at which the chirp signals are transmitted.
3) Presumming factor (PRESUM): a predetermined amount of frames can be coherently summed in order to reduce the data storage requirements of the instrument. This process necessarily reduces the information content of the acquired data, but tends to ensure that the resulting frame represents a good sample of the illuminated scene.

The resulting spatial distance can be obtained by:

$$\Delta x_a = \frac{PRESUM \cdot V}{PRF} \tag{14}$$

The scope of this part of the work is to assess how the variation of this parameter will affect the quality of the radargram, in terms of the possibility to detect subsurface dielectric interfaces.
For this purpose, a number of possible values for each parameter determining the spatial distance (V, PRF, Presum) were selected, according to the range of values that they will assume during the mission. This provides us with a set of possible Δx_a values.

Correction steps

Once a number of plausible spatial distance values has been selected we can proceed with the correction steps necessary to obtain the simulated radargram. Such steps are:

1) *Raw data correction:* we first need to apply some correction to the original raw data so that it mimics as faithfully as possible the data that would be acquired with the new Δx_a. We can reasonably assume that this parameters variation has no influence on the range distribution of power reflection: no correction to the original data will then be applied column-wise. The investigated raw data is then obtained by resampling each row of the analog data so that the resulting number of columns corresponds to the new Δx_a value. The resampling process is carried out by linearly interpolating the complex reflected signal values of each data row, according to the resampling factor, which is equal to the ratio $\Delta x_{a,I}/\Delta xa_{,A}$, where subscripts I and A indicate “investigated” and “analogue” respectively. Notice that this ratio can be smaller or greater than 1. The first case means we are upsampling the original data, the second case means we are downsampling it.
2) *Telemetry data correction:* the range and focusing processing requires, in addition to the reflected power data, a number of ancillary data describing the state of the satellite for each instant of signal transmission. This information comprises telemetry data such as spacecraft position, velocity, coordinates and distance with respect to the surface. Since this information is associated to each acquired frame, frame resampling automatically implies a resampling of these values. As done for the raw data correction, the investigated telemetry data is then obtained by linearly interpolating the analog telemetry data according to the $\Delta x_{a,I}/\Delta xa_{,A}$ ratio.
3) *Focusing:* Once the correct investigated raw data is obtained, we can proceed with raw data focusing in order to obtain the investigated processed data. As mentioned in Chapter 2, several focusing algorithms are available but focusing software is usually taylor-made for the specific mission and not publicly available. For this work, focusing was carried out using SOFA, a software developed by a former member of RSLab (*http://af-projects.it/sofa*). This software has been specifically designed for the SHARAD (SHallow RADar) data. More information will be given about SHARAD in chapter 6.

Simulated data is then obtained by first downsampling/upsampling the analog raw data and then applying range and azimuth focusing. While downsampling does not represent a problem from a theoretical point of view, data upsampling implicitly implies an increase in the information content of the radargram in terms of azimuth resolution. It is important to notice that applying the same corrections steps to the focused radargram would affect it in the same way in terms of resolution, but would have no effect in terms of SNR. Since what we want to evaluate is the ability of the focusing step to increase the target reflection's SNR (*focusing gain*), the methodology is compatible with theoretical constraints.

Chapter 5

Simulated data interpretation

As explained in the previous chapters, the general approach of this thesis consists in the correction of radar sounding data collected in a real analogous scenario in order to obtain useful simulated data of the investigated feature. The scope of this work is the creation of a simulated radargram database, whose interpretation can provide valuable information regarding the investigated feature (e.g. by ruling out some hypotheses on geoelectrical properties of the icy crust) and eventually yield useful guidelines for the future operation management and data analysis phases.

Several simulation, analysis and interpretation methods are currently available in the context of radar sounding, some of which have been briefly described in Chapter 2. Considering the outstanding flourishing in data analysis and image processing methods we are currently witnessing, supported by the rapid emergence of extremely powerful and robust artificial intelligence and machine learning tools among others, we can safely assume that, by the time the missions currently programmed to reach the Jupiter's system will be acquiring radar sounding data (i.e. early 2030s), our ability to interpretate radargrams will be drastically increased.

The purpose of this thesis is then twofold:

1) To carry out a preliminary analysis of available radar sounding data from analogous features in order to make predictions about the most important hypotheses on Jupiter's icy moons characteristics proposed in scientific literature so far, providing some practical tools to improve the future scientific return of the aforementioned missions to Jupiter's system.
2) To present a radargram database creation method that will constitute a resource for radar sounding analysis and interpretation tools that will emerge thanks to future improvements in radar sounding interpretation capabilities.

For what concerns the first purpose of the work, two main interpretation criteria have been devised. The rest of this chapter will be dedicated to the description of these criteria and of their application.

5.1 Similarity

Parameters and hypotheses

As introduced in *chapter 1* and *3*, a consistent part of the scientific research on Jupiter's icy moons aims at constraining their geological and geoelectrical characteristics in order to derive important information about their possible water content, in the form of subsurface brines or subcrustal oceans.

The geological description of the icy satellites is clearly a very complex operation and cannot be briefly carried out in an exhaustive manner. Nevertheless, a set of representative geoelectrical parameters can be chosen in order to define an overview of the satellite's characteristics. These parameters, together with the geological shape of the investigated feature and the instrumental parameters of the radar sounder, are the ones determining the final appearance of the recorded radargram. The selected parameters are preliminarily presented in Table 3 and will be described in detail in Chapter 6.

Similarity parameters
Bandwidth
Spacecraft height
Surface temperature
Temperature scale height
Void fraction
Impurity profile
Subsurface structure
Interface dielectric contrast

Table 3: List of selected parameters for similarity interpretation method.

For each of these parameters more than one hypothesis is possible and being able to define the correct value for each of them is the exact purpose of radar sounding investigation. We can then define an acquisition scenario and obtain a simulated radargram for each of all the combinations of parameter hypotheses, implementing the correction steps described in Chapter 4 to the original analog data.

Hypotheses discrimination

The first interpretation criterion is the ability of the radar sounder to distinguish between two hypotheses or combination of hypotheses. In fact, although the parameters by which we can describe the subsurface structure and geological properties are well explained in literature, we cannot assume *a priori* that all of them will have a strong impact on the radargram appearance. A theoretical determination of this impact is difficult, as it can be strongly dependent on the specific structure of the investigated feature. Moreover, particular combinations of hypotheses could compensate the effect of different parameters, making it impossible to distinguish their variation by analysing the acquired data.

It is then fundamental to understand which, among the selected parameters and resulting combinations of parameters, are more likely to produce a strong difference on the

geoelectric properties of the feature and on radargram appearance, in order to focus the radar sounding acquisitions on features in which those particular parameters are of crucial importance for the understanding of geological evolution and current state.

For this purpose, every simulated radargram needs to be compared with each of the other, quantitatively measuring the variation of information content and estimating the impact of the aforementioned parameters.

As explained in Chapter 4, the generation of the simulated radargrams first requires to define a geoelectrical model of the investigated feature by assigning a complex dielectric permittivity value to each pixel of the radargram. The comparison can then be carried out between two geoelectrical models, in addition to the comparison between simulated radargrams. This will allow to provisionally compare variations that solely depend on geoelectrical parameters and exclude the influence of instrumental parameters.

Mutual Information

We must then identify some appropriate tools that can quantitatively measure the variation between two radargrams. We selected Mutual Information (MI) as the most adequate quantity to express this variation. MI is a measure of the mutual dependence between two variables; in other words, it measures the amount of information that can be inferred about one variable by observing the other variable.

In the context of image comparison, MI has the property to provide a quantitative estimate of the variation in structure between two images. Moreover, in the specific case of radargram comparison, MI is not influenced by the total received power but only by its distribution across the image.

Since MI is not an intrinsically normalized measure, we have defined a normalized mutual information value as follows:

$$MI_{norm,ij} = \frac{MI_{ij}}{\sqrt{MI_{ii} \cdot MI_{jj}}} \tag{15}$$

so that the self information (i.e. the mutual information obtained by the comparison of a variable with itself) always equals 1.

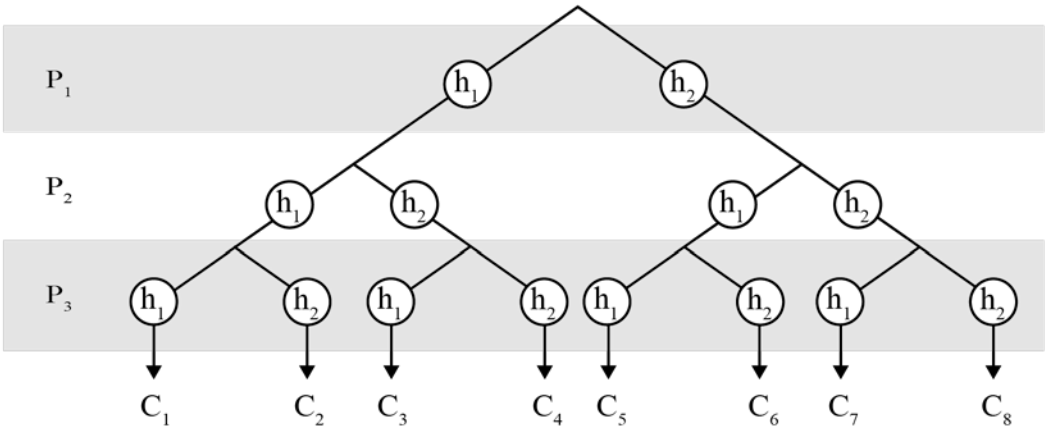

Figure 17: Schematic description of combination numbering, applied to a simple case with 3 parameters (P) and 2 hypotheses (h) each. This method allows to rapidly link a combination number to the relative hypotheses and to relate the discrimination matrix appearance to the underlying geological and geoelectrical meaning.

Discrimination matrix and visual interpretation

Once a quantitative measure of the similarity of each pair of radargrams has been computed, the result can be summarized through a discrimination matrix D. First of all an index must be assigned to each hypotheses combination. The element D_{ij} will then represent the value of MI_{norm} between radargrams corresponding to combinations *i* and *j*. The degree of similarity can then be visually represented by a colour grading representation, with colour intensity proportional to the MI_{norm} value. A brighter pixel will then correspond to a higher degree of similarity between two radargrams.

In order to be able to visually interpretate the discrimination matrix in $T(z) = T_s \cdot e^{\frac{z}{h}}$ an effective way, the combination indexing criterion must be selected in the appropriate way. In our case, a hierarchical indexing was selected: this means that the hypotheses combinations are successively divided into subsets, so that each subdivision corresponds to the variation of a single parameter. A visual explanation of this operation is illustrated in the tree diagram in Figure 17.

If a parameter variation produces a strong difference between radargrams or geoelectrical models, we will observe a pattern of blocks whose periodicity corresponds to the associated parameter subdivision. By sorting the order of parameters by which the combinations are subdivided, we will be able to understand their prominence (“hierarchy”) in revealing a visual pattern. The parameters producing a stronger variation can then be visually identified.

The proposed interpretation methodology based on the Mutual Information between radargrams can be applied regardless of the simulation steps necessary to obtain the investigated database and could then be useful both for pre-processed and raw data analysis. However, the generation of the discrimination matrix and its visual interpretation requires the database to have a significant number of elements; moreover, more than one parameter should be considered in order to produce the interpretation pool. In this specific work only the pre-processed data methodology respects these requirements.

5.2 Interface detectability

The main ability of radar sounders is to detect geological discontinuities through the reflection produced by dielectric contrast. This allows to visually represent a portion of subsurface in a faithful manner, except for the fact that the vertical dimension of the image represents time delays instead of actual distances. Although every ideal point target will produce an electromagnetic reflection of the transmitted signal, one of the main features investigated by this technology are dielectric interfaces. They appear in radargrams as horizontal lines underneath the surface.

Being able to maximize the intensity of the reflections in the acquired radargram is one of the main goals in radar sounding research, as it translates into the ability to identify with greater confidence the presence of interesting geological structures and retrace the evolution of planetary bodies characteristics.

Interface detectability is a particularly relevant interpretation criterion, as it is affected by all the major types of parameters treated so far: geoelectrical parameters (e.g.

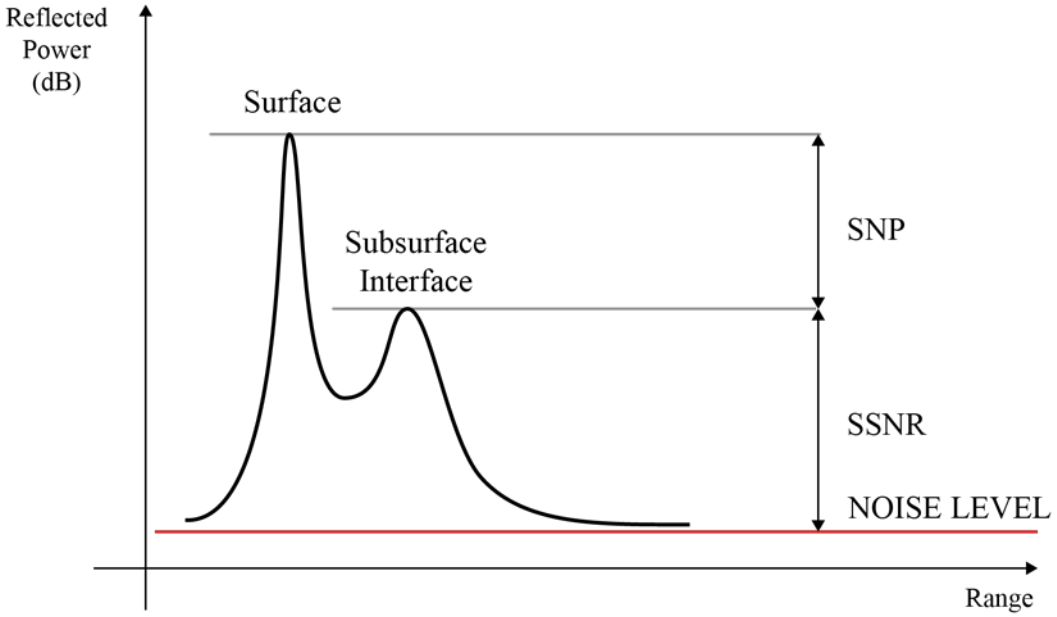

Figure 18: Simplified sketch of a typical range plot relative to subsurface interface detection. The graphical meaning of SNP and SSNR is showed.

dielectric contrast is determinant in the amount of reflected signal); instrumental parameters (e.g. spacecraft height, transmitted power and BW); data processing parameters (e.g. doppler compression contributes to increasing SNR).

In order to visually represent the distribution of signal reflection along the vertical dimension, a rangeline plot is usually drawn. In the case of interface detection, this is obtained by selecting an interval in which the putative interface is visible in the radargram. The selected radargram portion is then averaged row-wise in order to obtain a single vector representing the change in the reflected power with depth (see Figure 18). The power vector is then plotted in decibels as a function of time delay from transmission.

The interfaces with significant change in dielectric permittivity reflect a higher power according to Eq. 3, and thus appear as peaks in the range-line plot . The first peak from transmission corresponds to the surface reflection: it is generally the highest peak in the diagram, as the dielectric contrast between soil/ice and vacuum is usually the greatest. Successive peaks can be a hint of the presence of subsurface interfaces, but a careful analysis is necessary in order to confirm its presence.

There are two main difficulties in the reasearch of subsurface interfaces:

1) the artifacts deriving from clutter (explained in Chapter 2), that act similarly to an increase in noise power in the proximity of the surface.
2) the fact that no absolute power calibration is carried out for the instrument, making it inevitable to evaluate peak powers only in comparison with points of reference included in the acquired scene.

The solution of the first problem is considerably arduous without the development of sophisticated methods (see e.g. Ferro and Bruzzone, 2013) and is out of the scope of this work. Two main quantitative parameters were instead selected in order to cope with the second obstacle:

Subsurface SNR (SSNR): the power of each peak is compared with the radargram average noise value N. To compute N, a sample region above the surface is taken into account and its average power is calculated. This parameter is particularly appropriate to evaluate the ability of the focusing process to increase SNR.

Surface Normalized Power (SNP): the subsurface interface peak power is compared with the surface peak power. This allows us to evaluate the possibility to detect subsurface interfaces regardless of the noise power.

A visual representation of SSNR and SNP meaning is showed in Figure 18.

Chapter 6

Application to Ganymede

As mentioned in the previous chapters, the Jupiter system is the goal of an ESA's mission named JUICE, planned for launch on 2022. Among the selected payload, RIME will be the radar sounder that will allow to investigate the subsurface of the icy moons in order to characterize them in terms of geological and geoelectrical properties.

The main objective of RIME's investigation will be Ganymede, around which a circular orbit is planned during the second phase of the mission. For this reason, we selected a Ganymede's feature as investigated target. Conversely, the analog target is taken from Mars, for which a considerable radar sounding data is available and with which morphological similarities have been observed for several surface features.

Further investigation of RIME's capability to discriminate between different geoelectrical hypotheses and detect subsurface structures on Ganymede has gained an even greater importance considering the outstanding sounding depth (from 8 to 20 km) expected for this instrument (Heggy *et al.*, 2017).

In this chapter the main characteristics of the analog and investigated features selected for the application of the proposed methodology will be presented, including a presentation of the source data and a detailed description of the hypotheses selection, both in terms of geoelectric and instrumental parameters.

6.1 SHARAD and PDS database

The Mars Reconnaissance Orbiter (MRO) is a NASA mission launched in 2005, with the main objective of complementing the scientific investigation capabilities of the satellites already orbiting the planet. In addition to being an outstanding tool to advance our understanding of Mars formation processes and evolution, it contributes to the identification and characterization of future landing sites.

The six instruments onboard the satellite include three imaging systems, a visible-near infrared spectrometer, a thermal-infrared profiler and a shallow-probing subsurface radar sounder. The latter, named SHARAD (SHAllow RADar), is the instrument selected in this work as the source of analog radar sounding data. An overview of the MRO mission can be found in Zurek and Smrekar (2007).

SHARAD is a radar sounder provided by ASI (Agenzia Spaziale Italiana, the Italian Space Agency). Its main operating parameters are presented in Table 4. SHARAD has given a considerable contribution to the search for subsurface water ice Stuurman *et al*. (2016). Its sounding depth capabilities, mainly determined by it central frequency and bandwidth, are complementary to the Italian-US sounding radar Mars Advanced Radar for Subsurface and Ionosphere Sounding (MARSIS), which has recently provided very

Parameter	**Value**
Nominal science orbit altitude:	255-320 km
Extended/contingency orbit altitude:	230-407 km
Topographic margin:	-20/+10 km
Centre frequency:	20 MHz
Chirp bandwidth (*B*):	10 MHz
Pulse width:	85 microsecs
Receive window width:	135 microsecs
PRF (nominal):	700.28 Hz *
PRF (low orbit):	775.19 Hz *
PRF (high orbit):	670.22 Hz *
Radiated power:	10 W
Mass	
SEB (Electronics Box):	11.6 kg
Antenna + cabling:	5.5 kg
Power consumption	
Acquisition:	28W
Std-By:	13W
*) Can work with halved PRF	

Table 4: SHARAD's main instrumental parameters (Croci *et al.*, 2011)

strong evidence for the presence of a subglacial water lake on the southern hemisphere of Mars (Orosei *et al.*, 2018).

SHARAD's primary objective is to map dielectric interfaces down to depths of hundreds of meters, in order to characterize occurrence and distribution of expected materials. As highlighted by Seu *et al.* (2004), this investigation phase, in addition to directly contribute to the characterization of Mars geological properties, will allow to select appropriate landing sites for future on-ground exploration activities (such as drilling).

SHARAD data are made publicly available through the Planetary Data System (PDS). The PDS is an active archive created to distribute data acquired by NASA missions to the scientific community. All PDS datasets are peer reviewed and constantly updated and corrected.

The PDS data products used in this work are: EDR (Experiment Data Record), RDR (Reduced Data Record) and DEMs obtained from MOLA (Mars Orbiter Laser Altimeter) data.

EDR are the products containing the raw radar sounding data acquired by SHARAD, which in the context of this work represent the starting raw analog data of the simulation methodology described in Chapter 4. EDR data is subject to a limited amount of on-board data processing, namely: radial motion phase compensation, ADC, echo position tracking, pre-summing and compression. Notice that, although once uncompressed the raw data has the same dimensions of the pre-processed data, no visible trace of subsurface interfaces is present before the focusing process.

EDR data are correlated with the auxiliary information needed to locate observations in space and time and to process data further. The auxiliary data used in this work are spacecraft position, velocity, coordinates and receive window opening time. The latter represents the variable delay from transmission to acquisition, which accounts for the variability of the distance between the spacecraft and the surface.

RDR data consist in the EDR data to which a series of further ground processing steps have been applied (for details on RDR processing see Alberti *et al.*, 2007). This allows to work on data in which interface reflections are visible without further processing and contributes to reduce data storage requirements. The ground processing steps applied are: decompression and pre-summing, range processing, azimuth processing, relative

calibration (compensating for gain variations depending on spacecraft attitude and position of large moving parts such as solar panels), ionospheric correction and time alignment of echoes. These processing steps (except for ionospheric correction) are the same carried out in the raw data methodology using SOFA.

Although not strictly necessary for the processing involved in the methodology of this thesis, the software used for the simulations requires a description of the investigated area topography, in the form of a DEM. This data is made available by MOLA, a laser altimeter operating in orbit from 1997 to 2001, and can be download from the PDS database as well.

6.2 Pedestal craters

The selection of the investigated feature has been based on geomorphological considerations, supported by the state-of-the-art analysis of the images provided by the Voyager and Galileo missions (Patterson *et al.*, 2010).

A brief introduction on Ganymede's main geomorphological features has been provided in Chapter 1, in which the importance of impact and cratering phenomena has clearly emerged.

The Ganymede's features selected for the application of the proposed method are pedestal craters. Pedestal craters are particular types of recently formed impact craters surrounded by ejecta blankets that end with sharp terminations. These impact craters are distinguished by the fact that both the crater pit and the ejecta rise above the surrounding surface. It appears from Voyager images that pedestal craters morphology is partially unrelated with surrounding grooves, from which we can deduct that ejecta deposit have overlapped preexisting topography.

Craters with similar morphology can be observed on Mars. A comparative analysis of pedestal craters on Mars and Ganymede can be found in Horner and Greeley (1982).

Among Jupiter's icy satellites, Ganymede is the one in which the largest number of preserved large pedestal craters on relatively flat surface terrain is present. Two types of geological formations (facies) usually characterize this particular feature: an inner pedestal facies (IPS) with a roughly circular outer edge rising about 100 m above the surrounding surface; an outer radial facies (ORF) characterized by granular textures and radial flutings. Analyses of the images made available by Voyager mission seems to

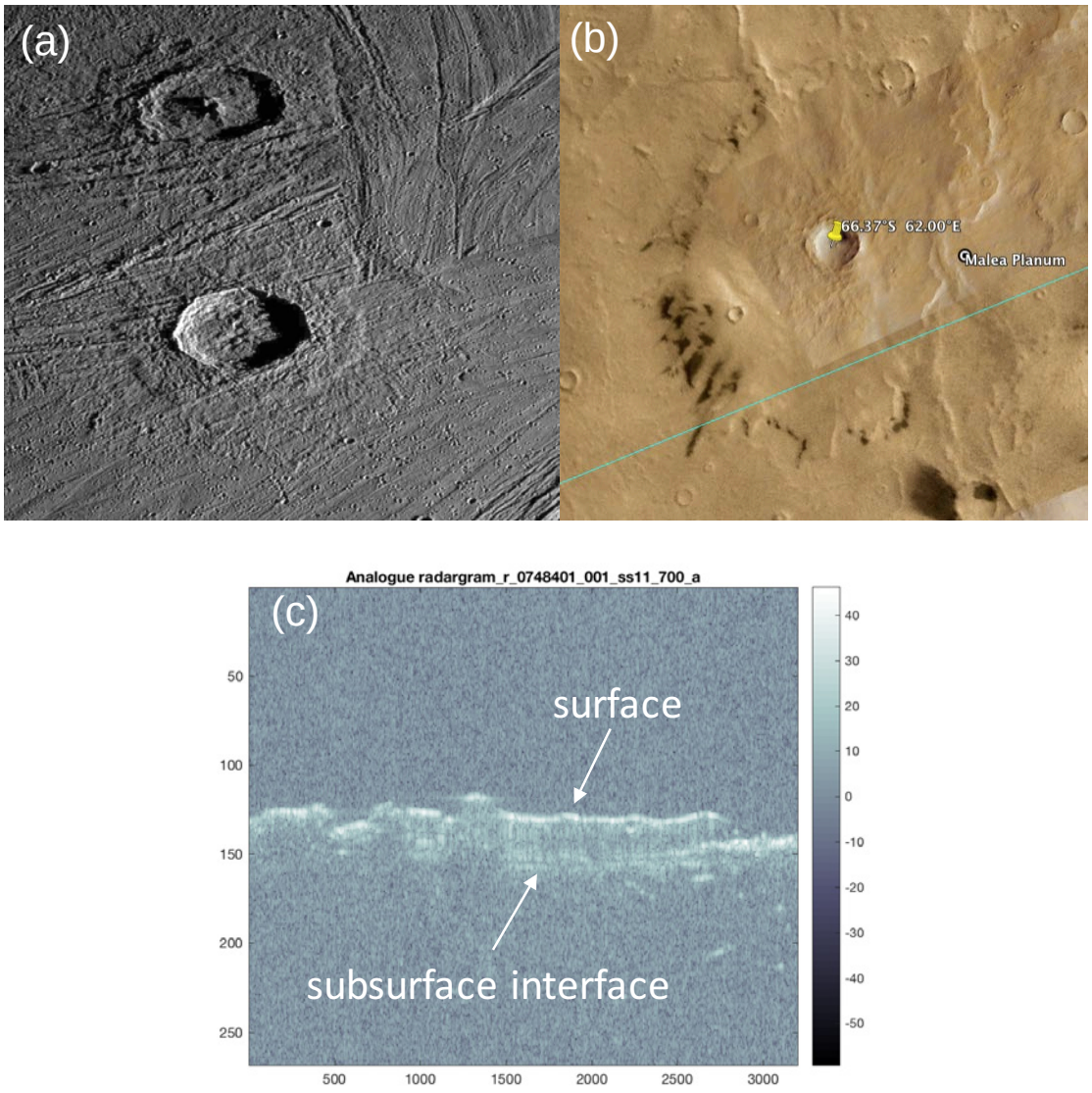

Figure 19: a) Image by Galileo of a pedestal crater on Ganymede, a representative example of the investigated feature. b) Image of the selected analog pedestal crater on Mars; the blue line represents SHARAD's ground track. c) Original radargram of the selected analog pedestal crater.

show a well defined relationship between the diameters of the outer edge of the ejecta deposit and of the crater rim. Moreover, the hypothesis of self similarity, which predicts that ejecta deposits scale with crater diameter in the same way, seems to hold.

A comparative analysis between ejecta on icy satellites has been carried out for example in Schenk (2002).

A great number of impact craters have been observed on Mars as well, including pedestal craters (Barlow, 2006; Nunes *et al.*, 2011). A wide variety of ejecta

morphology have been identified there, among which the layered type seems to be the most common, with the number of layers varying from 1 to more than 3. Pedestal craters formation process is not yet clearly understood and, although dedicated studies should be carried out according to the specific environment, a comparison between pedestal craters on different planetary bodies could lead to a better understanding of the formation phenomena involved. Two major formation models have been proposed, one suggesting impact on near-surface volatile reservoirs while the other involving the interaction between ejecta and the thin atmosphere of Mars. Similar formation hypotheses can be applied to Ganymede but in this case a smaller influence of the atmosphere interaction is predicted. The absence of central crater pits on planetary bodies with a low presence of volatile materials (like the Moon) shows that central pits are not solely due to the cometary impacts, suggesting instead that high temperature vaporization of volatiles under the center of the transient crater could be a primary cause of their formation. Conversely, the outer shape of the pedestal is probably a combined consequence of eolian erosion of the surrounding material and some sort of armouring mechanism provided by impact melting (Barlow, 2006). Pedestal craters on Mars are particularly interesting because of their possible relation to water ice reservoirs and source of geological traces of martian climate change.

Since the analysis of planetary geological characteristics is usually based on remote sensing investigations, the choice of an adequate analog feature has to rely on the comparison of observable geophysical signatures. In fact, most of the planetary geology investigation is base on the assumption that similar subsurface structures will be linked to similar surface expressions. The choice of Mars as the source of analog data is then supported by the geomorphological similarity between pedestal craters on Ganymede and Mars. Moreover, although no quantitative estimate of the homologous temperature of the analog and investigated targets has been carried out, this selection criterion is theoretically consistent considering that homologous temperatures are expected to be comparable, allowing to cope with the radical difference in composition and absolute temperatures.

6.3 Selected analog feature

The selected analog feature for radargram simulation is a pedestal crater located in the Malea Planum, a volcanic plateau on the southern hemisphere of Mars (coordinates 66.37 S, 60.00 E). The pedestal is about 89x115 km, while the crater rim has a diameter of 14.5 km. The ratio between pedestal and crater mean diameter is more than twice the mean of the entire pedestal population. This pedestal crater was interested by more than 30 SHARAD passages, some of which were specifically dedicated to the investigation of this feature. Nunes *et al.* (2011) carried out a comparison between radargram 748401 and computational simulated clutter of the same ground portion, based on MOLA DEM (see Chapter 2 for details on clutter analysis). This investigation showed that some weak echoes underneath the pedestal surface do not appear on the cluttergram, suggesting that those reflections are a sign of the presence of a dielectric interface.

In order to be able to simulate the investigated radargram, a geoelectrical model has to be defined for the analog feature. This means that we have to associate a dielectric permittivity value to each point of the feature. A geoelectrical characterization of the selected pedestal crater was carried out by Nunes *et al.* (2011). The basic assumption of that work is that the thickness of the material between the surface and the subsurface interface is the same as the height of the pedestal above the surrounding surface. This implies that the subsurface interface forms a quasi-continuous layer with respect to the surroundings. Since the vertical dimension of the acquired radargram represents delay time, subsurface interface and surrounding surface do not appear in line on the radargram, because electromagnetic signals travel faster through vacuum. When converting the radargram from time domain to depth domain, the depth of the interface will depend on the assumed dielectric permittivity. The dielectric permittivity value for which the assumption is respected will be selected. Following this method, a bulk permittivity value of 4.5±0.5 was derived.

6.4 Investigated feature hypotheses

A series of representative parameters have been selected for the investigated feature and are showed in Table 5. In the first part of this section these parameters and the relative hypothetical values will be illustrated. Then we will proceed with presenting the

Geological hypothesis	Mars Analogue Pedestal craters			
Instrument parameters	Bandwidth	LRO	HRO	
	Spacecraft height	500 km	200 km	
Geophysical hypotheses	Surface temperature	80 K	100 K	200 K
	Scale height	Constant base	Constant slope	
	Void fraction	0.01	0.1	0.2
	Impurity profile	Dark terrain	Bright terrain	
Geo-electrical hypotheses	Structure	Continuous	Discontinuous	
	Epsadd	-0.8	0.8	

Table 5: Selected parameters and relative hypotheses

equations that allow us to define a geoelectrical model starting from these parameters. Hypotheses selection was mainly carried out following the works of Heggy *et al.* (2017) and Bruzzone *et al.* (2013).

Pre-processed data methodology

- **Spacecraft height**: RIME's operations will go through a first series of flybys of the icy satellites and a successive phase in orbit around Ganymede. The orbital design of the mission established a spacecraft height above the surface of 500 km during the orbiting phase. Compatibly with fuel availability in the later stages of the mission, spacecraft height could be decreased to 200 km. These two hypothetical values were then selected.
- **Bandwidth**: this parameter is one of the main factors influencing the final range resolution of the instrument. Two resolution modes were selected for the mission during the design phase: *low resolution* and *high resolution*, corresponding respectively to a 1 MHz and 2.8 MHz bandwidth. Low resolution mode will be used to reduce data volume when observing deep targets.
- **Surface temperature:** information on Ganymede's surface temperature is mainly derived by spectrometric and radiometric observations. Surface temperatures vary from 90 K at night to 150 K during the day, with an expected average value of 120 near the equator (Heggy *et al.*, 2017). This range has been slightly extended in order to take into account the temperature variation between the equator and the poles. Three values were then selected: 80 K, 100 K and 120 K.

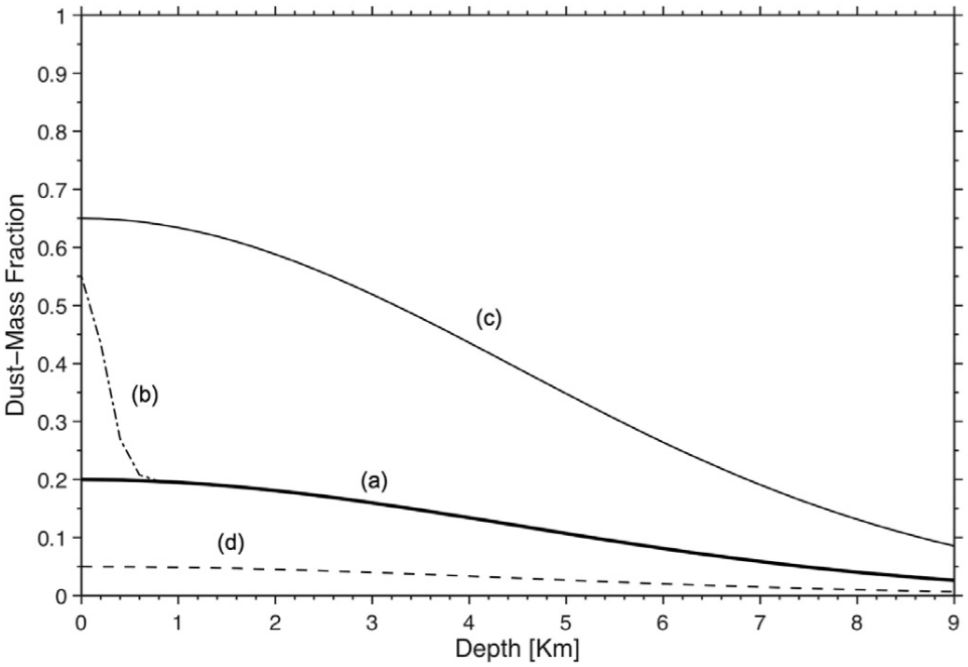

Figure 20: Impurity distribution for a) Ganymede's bright terrain, b) Ganymede's dark terrain. Callisto (c) and Europa (d) impurity distributions are showed for comparison. (Heggy *et al.*, 2017)

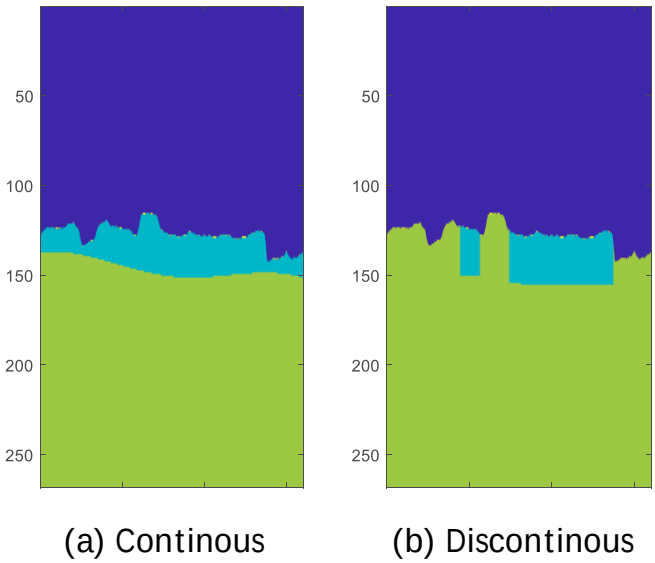

Figure 21: Illustration of the difference between continuous and discontinuous structure hypothesis (Thakur and Bruzzone, 2019)

- **Scale height:** a purely conductive heat transfer model is generally proposed in literature for Ganymede literature, which translates into an exponential temperature distribution:

$$T(z) = T_s \cdot e^{\frac{z}{h}} \quad (16)$$

where T_s is the surface temperature, z is the depth and h the scale height. Two hypotheses are considered in this work for determining the scale height, i.e. a constant base temperature 130 K or a constant slope.

- **Void fraction:** the shallow crusts of icy satellites are brittle and constant exposure to impacts and tidal stress is probably responsible of frequent ruptures. For this reason, a certain amount of porosity is envisaged. For Ganymede, a 10% porosity fraction is proposed in literature. In order to take into account the possibility of particularly compact or ruptured material, three hypotheses for the porosity fraction are considered here: 0.01, 0.1 and 0.2.
- **Impurity profile:** two main terrain types are observed on Ganymede: bright terrain (BT) and dark terrain (DT) (more details are given in Chapter 1). One of the main features distinguishing the two types is the impurity content and distributions. For BT, a gaussian distribution of dust mass fraction is hypothesized, with a surface value of 15%. The same model is applied to the DT, with an additional regolith layer in the first hundreds meters, increasing the surface value to 55%. Impurity distribution is showed in Figure 20, together with Europa and Callisto distributions for comparison.
- **Dielectric contrast:** the state-of-the-art characterization of pedestal craters predicts that the ejecta deposit material and the underlying material have different compositions and thus different dielectric properties. This difference is what produces the radar reflections at the interface between the ejecta and the substratum, which appear on radargrams as bright horizontal lines. To simulate this dielectric contrast, an additional real dielectric permittivity component has been added to the permittivity obtained for the substratum. Since the ejecta permittivity could be higher or lower, two representative values were chosen: +0.8 and -0.8.

- **Structure:** the interface reflections observed on radargrams in correspondence to the pedestal crater base do not always appear continuous throughout the feature. On the contrary, interruptions can be sometimes observed, usually around the center of the pedestal. It is not yet clear if these interruptions are due to the limits of the instrument or to an actual discontinuity in the pedestal structure. Two hypotheses were then considered: ‘cont’, i.e. dielectric contrast applied throughout the feature, above the pedestal base; ‘discont’, i.e. dielectric contrast applied only above visible interface. A visual representation is presented in Figure 21.

For each combination of the aforementioned hypotheses, a geoelectrical model can be defined specifying a complex dielectric permittivity value for each pixel of the radargram. Dielectric permittivity values for water ice can be obtained as a function of temperature, porosity and impurity concentration as follows (Heggy *et al.*, 2017).
Dielectric permittivity can be expressed as a complex number $\varepsilon = \varepsilon' + i\,\varepsilon''$, where:

$$\varepsilon' = \varepsilon_\infty + \frac{\varepsilon_0 - \varepsilon_\infty}{1 + \omega^2 \tau^2} \tag{17}$$

and

$$\varepsilon'' = \frac{\omega\tau(\varepsilon_0 - \varepsilon_\infty)}{1 + \omega^2 \tau^2} \tag{18}$$

Here ω is the angular frequency, τ the relaxation time, ε_0 and ε_∞ are the low and high permittivity limits.
To take into account the contribution of porosity and impurities to the dielectric permittivity, the Rayleigh multiphase mixing formula is applied:

$$\varepsilon_{eff} = \varepsilon_e + 3\varepsilon_e \frac{\sum_{n=1}^{N} f_n \frac{\varepsilon_{i,n} - \varepsilon_e}{\varepsilon_{i,n} + 2\varepsilon_e}}{1 - \sum_{n=1}^{N} f_n \frac{\varepsilon_{i,n} - \varepsilon_e}{\varepsilon_{i,n} + 2\varepsilon_e}} \tag{19}$$

Velocity (m/s)	PRI (μs)	Presum	Δx_a (m)
1900	2500	1	4.75
1900	2500	2	9.5
1900	2500	4	19
1900	5000	1	9.5
1900	5000	2	19
1900	5000	4	38
3200	2500	1	8
3200	2500	2	16
3200	2500	4	32
3200	5000	1	16
3200	5000	2	32
3200	5000	4	64

Table 6: List of all the possible hypotheses combinations for raw data methodology. The combinations selected for the simulation are framed in red.

where ε_e is the permittivity of water ice, while f_n and ε_n are volume fraction and permittivity of the n-th phase of the mixture. The phases mixed to water ice in this case are dust (representing impurities) and void space (representing porosity). Dielectric permittivity values for impurities are obtained by Heggy *et al.* (2017), in which it is assumed that contaminants are due to ions transferred from the Jovian magnetosphere, grains coming from Io or due to meteoroid and comet impacts.

Raw data methodology

In the second part of the work, no modelling of the geoelectrical properties of the feature was involved. Conversely, the impact of orbital and instrumental parameters on the focusing process was analysed, in terms of the influence of azimuth spacing (Δx_a) between acquisitions. The parameters determining Δx_a and the selected hypothetical values are:

- **Spacecraft velocity**: as mentioned before, JUICE will go through a first flyby phase and a successive orbiting phase around Ganymede. In order to represent the possible variability of spacecraft velocity, two extreme values were selected: 1900 m/s and 3200 m/s.

- **PRF**: RIME's PRF value can be changed in order to adapt to data rate and sounding depth requirements. In fact, the data volume for a radargram is proportional to PRF. The selection can be made between 200 Hz and 400 Hz, corresponding to a PRI (Pulse Repetition Interval) of 2500 μs and 5000 μs respectively.
- **Presum**: in order to reduce further the data volume for a specific radargram, a specific number of successive frames can be coherently summed onboard. The number of presummed frames for RIME can be 1, 2 or 4.

The Δx_a value for each combination is obtained from Eq. 14.

By considering all the possible combinations of these hypotheses (see Table 6) we observe that only one of them yields a Δx_a value grater than SHARAD's Δx_a. We then take into account three possible values for Δx_a, i.e. 32, 39 and 64 m. The three values correspond respectively to the downsampled, original (SHARAD) and upsampled cases.

Chapter 7

Results

In this chapter the first results of the application of the the proposed methodology will be presented. The chapter is divided into two main sections.

In Section 7.1, relative to the elaboration of pre-processed radar sounding data, the impact of geoelectric and instrumental parameters on investigated radargrams will be discussed. Quantitative and qualitative considerations will be presented in terms of the predicted ability of the instrument to 1) discriminate between different hypotheses and 2) identify subsurface interfaces.

In Section 7.2, relative to the elaboration of raw radar sounding data, the influence of instrumental and orbital parameters on the focusing process will be discussed. The variation of radargram quality will be presented in terms of subsurface detection capability, similarly to what done in the first section. Some further considerations will be made about the visual comparison of simulated radargrams.

7.1 Pre-processed data

Hypotheses discrimination

The ability of a radar sounding instrument to discriminate between several hypotheses regarding a specific geoelectric parameter is directly correlated to its capability to characterize the composition of icy planetary bodies. Moreover, it is necessary to understand whether the variation of specific instrumental parameters can enhance the instrument's potential or, on the contrary, undermine its scientific return.

Geoelectrical models comparison

The methodology described in Chapter *5* was first applied to the simulated geoelectrical models. This allows us to first treat geoelectrical and instrumental parameters separately, in order to discriminate between the patterns that depend on the nature of the investigated feature and those that are specifically due to the instrument design.

A number of tentative rearrangements of the matrix have been tried, searching for any visible recurring patterns in the matrix and comparing it with the order in which the parameters had been sorted. In Figure 22, the matrix resulting from the following order of parameters is presented: impurity profile, void fraction, surface temperature, subsurface structure, temperature profile, dielectric discontinuity.

Observing the discrimination matrix in Figure 22, several interesting conclusions can be drawn:

- Impurity appears to be the easiest parameter do discriminate. We can see that comparing geoelectric models referred to BT and DT with models of the same type typically yields high values of mutual information. On the contrary, the comparison of geoelectric models with different impurity profiles results in low values of mutual information.This result is particularly interesting, as being able to relate the surface appearance of a geologic type (i.e. BT or DT) to the actual subsurface composition (impurity profile) is one of the main objectives of RIME (Cofano *et al.*, 2015).
- In case of DT, impurity influence is so prominent that other parameters almost result indistinguishable.

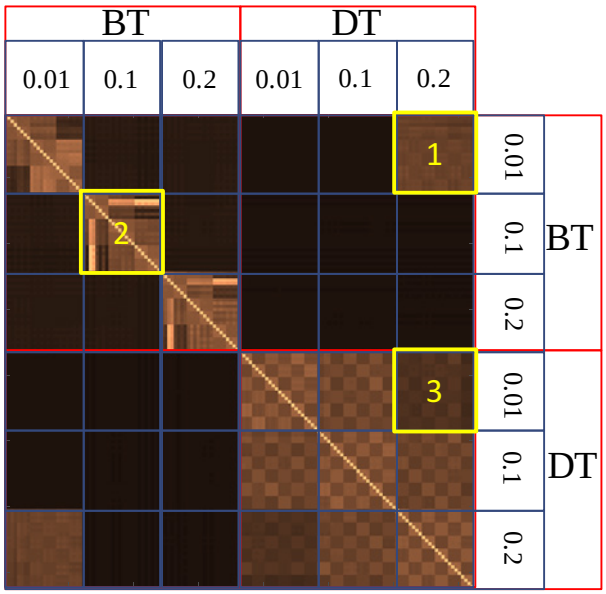

Figure 22: Discrimination matrix relative to geoelectrical models comparison. See text for discussion.

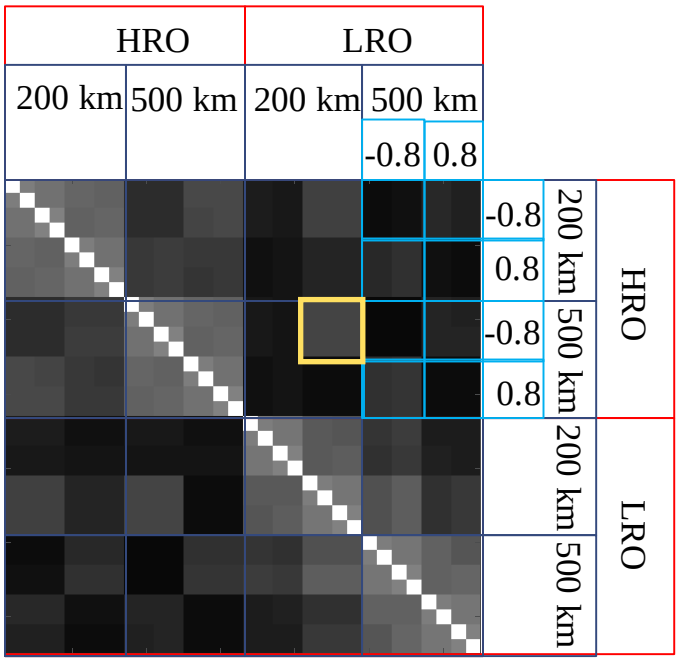

Figure 23: Discrimination matrix relative to radargram comparison. See text for discussion.

- Among BT combinations, void fraction seems to play an important role on the geoelectrical model structure, as models with different porosity show considerably low mutual information values. This is particularly interesting because it highlights a fundamental difference between BT and DT response to radar sounding investigation.
- Complex interdependence patterns emerge among BT models with the same porosity values (see box 2). This suggests that, except for porosity, in case of BT no single parameter has a predominant role in the determination of the geoelectrical properties, as far as visual analysis can show. Clustering methods could be a useful tool to highlight further interdependence patterns which are not clearly visible.
- Box 1 represents an example of compensation between the variation of multiple parameters. In fact, comparing geoelectric models with different impurity distribution generally yields small mutual information values. In this particular case, though, the simultaneous variations of impurity (BT vs. DT) and porosity (0.01 vs. 0.2) compensate for each other. In other words, the simultaneous variation of parameters which intrinsically lead to strong geoelectrical model variations could paradoxically result in less distinguishable models.

Radargrams comparison

The same methodology was applied to the direct comparison of radargrams. In this case, the combination of all the hypotheses was taken into account, resulting in more complex patterns (see Figure 23).

As for the geoelectric models comparison, some important conclusions can be drawn:

- RIME's resolution mode (LRO, HRO) appears to be the most important parameter determining the final radargram appearance.
- Spacecraft altitude seems to be the second most important parameter.
- The compensation phenomenon is particularly evident here. For example, the elements contained in the yellow box in Figure 23 represent the comparison between radargrams with different bandwidth, spacecraft height and contrast but result in a relatively high mutual information value.

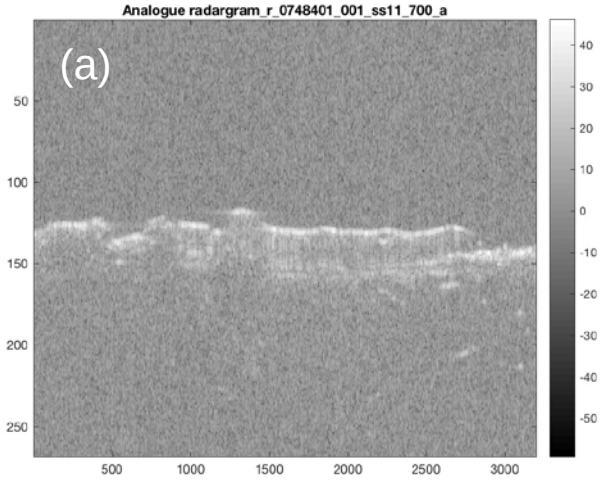

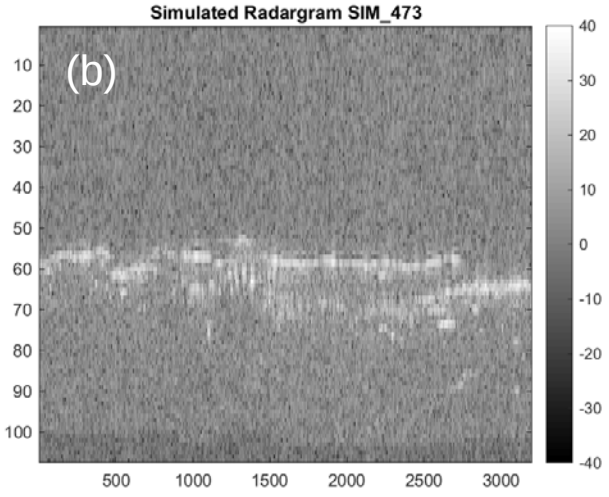

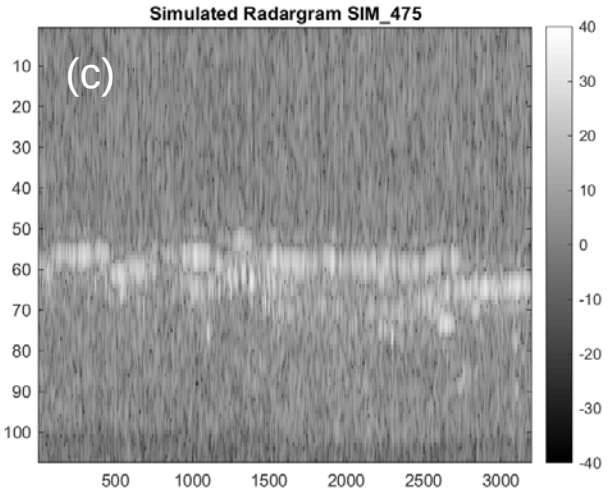

Figure 24: Comparison between original radargram (a) and two very different radargrams in terms of mutual information (b and c).

Visual comparison

Besides the computational interpretation methods described in Chapter 2 and the tools that will be developed in the future thanks to emerging disciplines like artificial intelligence and machine learning, radargram interpretation has strongly relied so far on the planetary scientists' experience and ability to visually identify interesting features.
In Figure 24 a comparison between the original analog radargram and two simulated radargrams with a particularly low mutual information value is presented. In this case resolution mode (LRO, HRO) is the only parameter that varies between the two simulated radargrams. This comparison shows that the particular morphology of the feature and the interface horizon, which are clearly visible on the analog SHARAD radargram, is still evident on the HRO simulated radargram but almost indistinguishable on the LRO simulated radargram.
From this comparison we can see that the proposed methodology, besides being a powerful tool for the creation of databases dedicated to automatic interpretation, has a great potential to provide simulated data for timely qualitative interpretation that could be useful in the decision making process during the operative phase.

Subsurface detectability

As explained in the previous chapters, the ability of a radar sounder to highlight subsurface interfaces is of fundamental importance for the characterization of icy moons and planetary bodies in general. Here we present the first results of the radargrams comparison in terms of subsurface interface detectability with respect to noise power and surface reflection power.

SNP

The first interpretation parameter is the ratio between subsurface interface reflected power and the surface reflected power. A plot of SNP value for each simulated radargram is showed in Figure 25. From this plot we can observe that combinations are divided into two well separated clusters. The parameter that differentiates the two clusters and that seems to produce the greatest difference in this regard is the dielectric contrast between the ejecta material and the ground ice underneath the pedestal crater

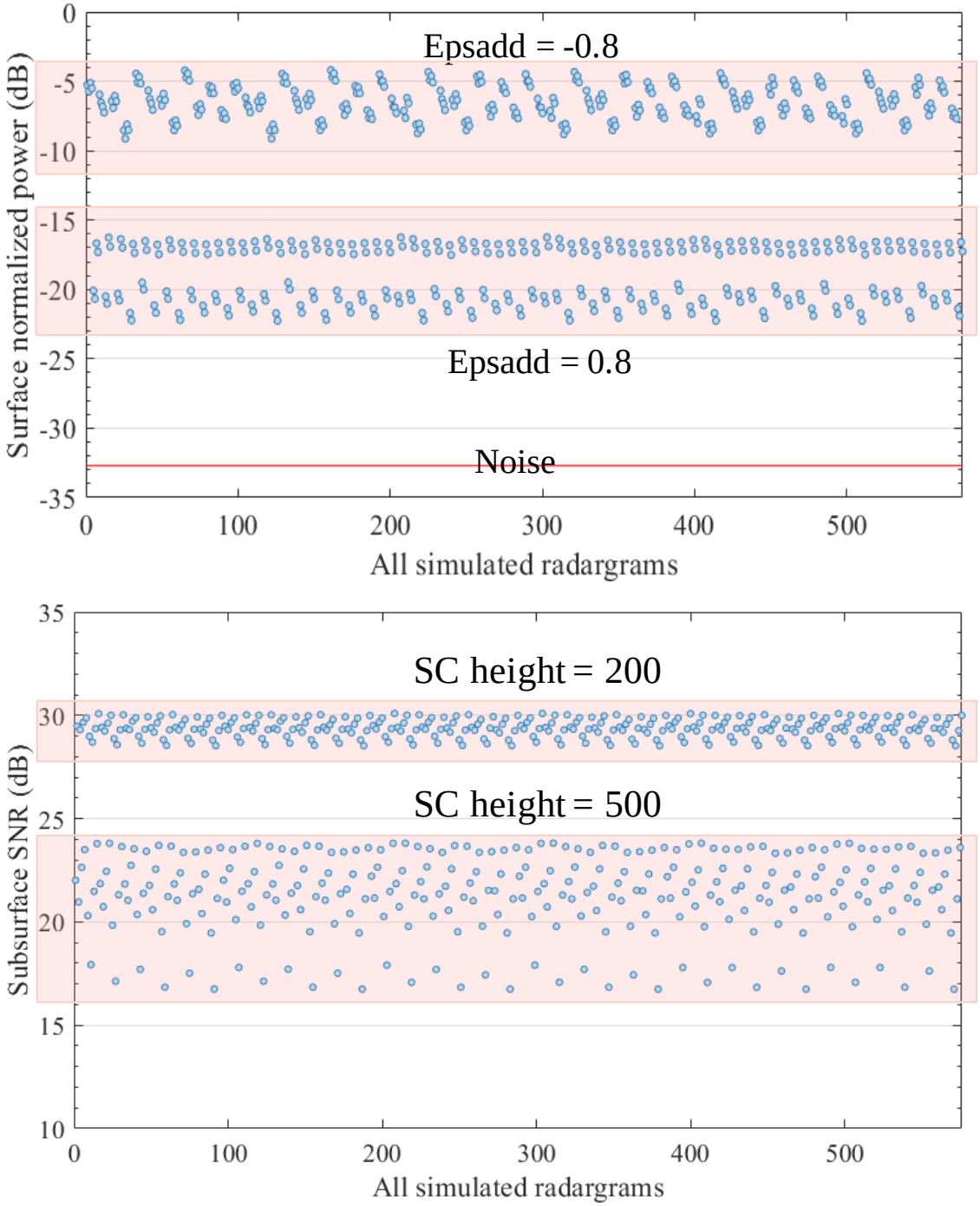

Figure 25: Above: plot of the SNP value for all the hypotheses combination. Below: same for SSNR.

base. In particular we observe that SNP is greater when the dielectric permittivity of the ejecta is lower (-0.8) than the underlying material.

From a geological point of view, this result confirms theoretical predictions suggesting that a clearly visible subsurface interface trace on the radargram is a sign that pedestal and underlying materials are well differentiated, possibly due to a lower level of contamination of the material exposed as an effect of the impact.

SSNR

The second interpretation parameter is the ratio between subsurface interface reflected power and noise power. A plot of the SSNR value for each simulated radargram is showed in Figure 25b. Similarly to the previous case, two separated clusters are visible on the plot. Here the main discrimination parameter between the two clusters is the spacecraft altitude. This result confirms theoretical equations predicting that target reflections power is inversely proportional to the squared distance from the target. Since noise power level is the same for the two clusters, the results are coherent with theoretical predictions.

Although the subsurface interface reflection power is well above the noise threshold for all the simulated radargrams, the increase in SSNR provided by a lower orbit could be crucial for targets which are less differentiated or in which the presence of an interface cannot be confirmed by a higher altitude acquisition.

We can further observe that SSNR values vary in a wider range for 500 km radargrams, suggesting that some other parameter or combination of parameters could have a strong impact in interface detectability. Further analysis should be carried out in this regard.

7.2 Raw data

The main object of investigation for the second methodology is the influence of the focusing process in our ability to identify subsurface interfaces in the acquired radar sounding data.

In the proposed methodology, the azimuth distance Δx_a between two successive acquisitions is the only varying parameter. For this reason, no analysis based on hypotheses combinations is carried out.

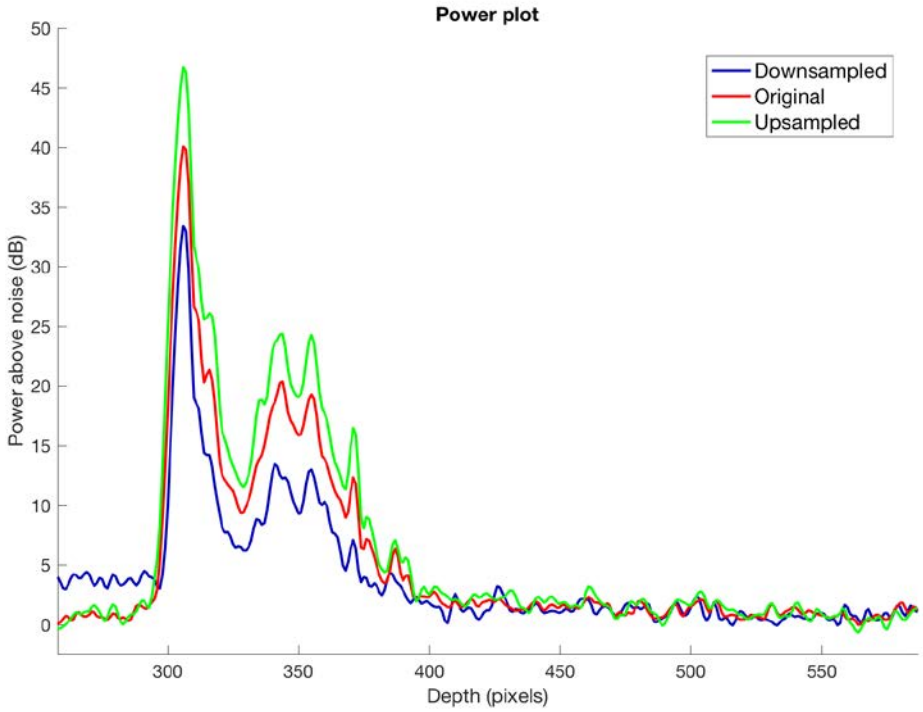

Figure 26: Range plots for the original, upsampled and downsampled simulations.

	SNP (dB)	SSNR (dB)
Downsampled	-21.97	11.45
Original	-22.55	17.45
Upsampled	-25.17	21.52

Table 7: SNP and SSNR values for downsampled, original and upsampled simulations.

The power distribution of the reflected signal is represented in Figure 26, normalized with respect to noise threshold. As visible on these power plots, the identification of a single subsurface peak value for quantitative analysis is not always possible. This could be either due to a gradual variation of dielectric properties with depth (low level of differentiation), to the presence of multiple interfaces and to the noise introduced by clutter. Nevertheless, the bulk peaks relative to surface and subsurface reflections are clearly visible. In particular, two prominent spikes can be observed on the subsurface bulk peak. In this work, we have decided to consider the higher spike as the reference

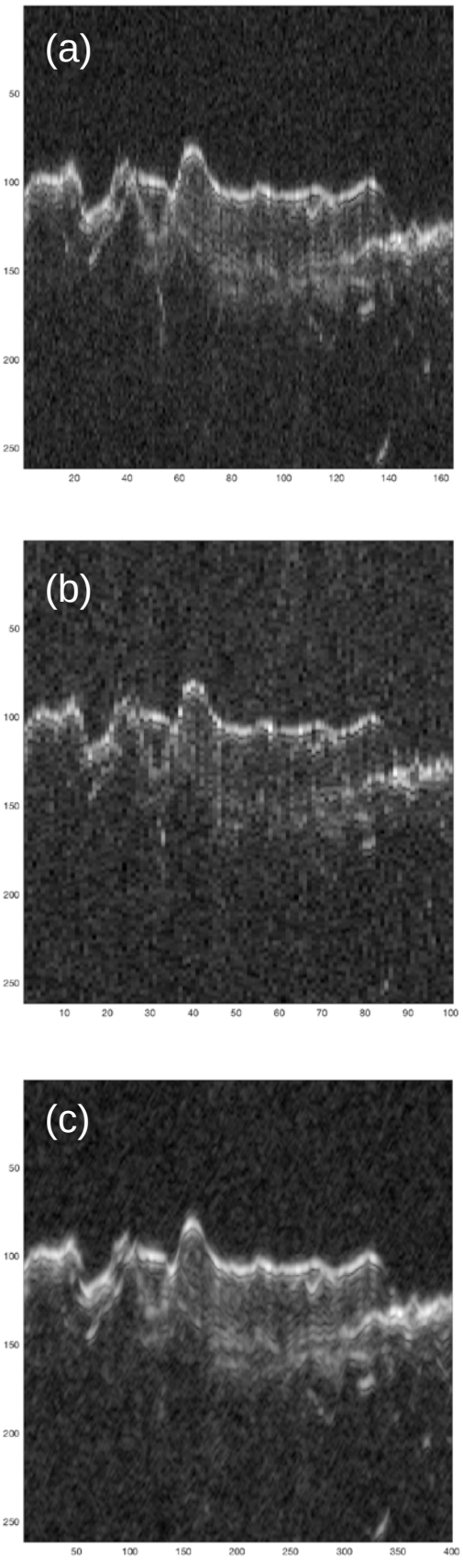

Figure 24: Comparison of radargrams relative respectively to original (a), downsampled (b) and downsampled (c) data.

subsurface reflection power.

As done for the first proposed methodology, a visual comparison between the simulated radargrams is shown in Figure 27.

SSNR

As explained in Chapter 6, three Δxa values have been selected, respectively representing the downsampled, original and upsampled simulated raw data. Observing the power plot in Figure 26, it is clearly visible that SNR value for both the surface and the subsurface interface increases as Δxa decreases. This mainly translates into an increased potential to identify subsurface interfaces and confirms theoretical predictions about the property of azimuth focusing to increase SNR of reflected signal. The SSNR value for each of the simulated cases is shown in Table 7.

From an operational point of view, reducing Δxa implicates at the same time an increase in data storage and transmitted power requirements. The choice of an adequate Δxa value (i.e. of an adequate combination of PRF and presumming factor) will then be the result of a trade-off between scientific requirements and technical constraints.

SNP

A similar comparison between downsampled, original and upsampled simulated radargrams has been carried out in terms of SNP. The SNP value for each of the simulated cases is shown in Table 7. We can observe that SNP slightly increases in the downsampled case, while it considerably decreases in the upsampled case. This behaviour seems to show that decreasing Δx_a has a non-linear impact on the ability of the azimuth focusing process to increase SNR, as the radargram power of targets with a higher dielectric contrast (surface) is increased more than targets with a lower dielectric contrast (subsurface interface). Since the variations in SNP are relatively low and few simulations were produced, the methodology should be applied to a larger number of analog data and Δx_a values in order to confirm the result with statistical significance.

Chapter 8

Conclusions

Radar sounding is one of the most promising technologies for the exploration of icy moons. RIME (Radar for Icy Moon Exploration) is a radar sounder that will be launched to the Jupiter system in 2022 with the principal aim of characterizing Ganymede as a planetary object and assess its habitability.

The main objective of this work has been the investigation of the influence of geoelectrical, instrumental and data processing parameters on RIME's ability to discriminate between different compositional hypotheses and to detect potential subsurface features.

In the first part of the work, a recently proposed method based on the exploitation of data collected on analog geological features was selected. For this purpose, a set of hypotheses combinations were used to correct a radargram relative to a pedestal crater located on the southern hemisphere of Mars, in order to produce simulated radargrams of potential pedestal craters on Ganymede.

In the second part of the work, a different methodology was developed to obtain simulated radargrams by correcting the raw data (i.e. before range and doppler

focusing) of the same Mars feature, in order to assess the influence of the focusing step on RIME's feature detection capabilities.

A series of interesting results have been obtained in terms of hypotheses discrimination. Impurity, which is the main parameter that distinguishes Ganymede's dark and bright terrain, appears to be the easiest hypothesis to discriminate. A good discrimination capability has been also found for void fraction, limitately to bright terrain. Complex patterns of hypotheses interdependence and hypotheses compensation have been observed when taking into account other parameters and should be further investigated.

For what concerns subsurface interface detectability, spacecraft height and dielectric contrast seem to be the most prominent parameters, confirming theoretical predictions. Moreover, the application of the raw data methodology showed that reducing the azimuth spacing between successive acquisitions could provide a significant improvement in the ability of the focusing process to increase the SNR of the subsurface interface reflected signal.

These results confirm the potential benefits of the proposed methodology in several aspects. In terms of scientific investigation, this method could 1) support geoelectrical inversion investigation aimed at characterizing the geoelectrical properties of icy moons subsurface and 2) provide radargram databases for the training of automatic interpretation algorithms. Moreover, the proposed methodology could be of great support during the design and operation management phases, helping to identify high priority targets and selecting the appropriate instruments parameters for the investigation of specific features.

Some of the results of this work have contributed to the writing of a paper (Thakur *et al.*, 2019) that will be presented at the 2019 International Geoscience and Remote Sensing Symposium (IGARSS).

As future work, the application of this method to a higher variety of Ganymede features could be taken into account, in order to test its capabilities in different operating conditions. The use of clustering algorithms could be also considered to help recognize interdependence patterns that are difficult to discern visually. Finally, the method should be further developed in order to take into account the impact of Jupiter electromagnetic noise on the radargram appearance.

Bibliography

Aglyamov, Y., Schroeder, D. M. , Vance, S. D. Bright prospects for radar detection of Europa’s ocean. Icarus 281, 334–337 (2017).

Alberti, G., Dinardo, S., Mattei, S., Papa, C. & Santovito, M. R. SHARAD radar signal processing technique. in 2007 4th International Workshop on, Advanced Ground Penetrating Radar (IEEE, 2007). doi:10.1109/agpr.2007.386564

Anderson, J. D., Lau, E. L., Sjogren, W. L., Schubert, G. & Moore, W. B. Gravitational constraints on the internal structure of Ganymede. Nature 384, 541–543 (1996).

Anderson, J. D. Europa’s Differentiated Internal Structure: Inferences from Four Galileo Encounters. Science 281, 2019–2022 (1998).

Barlow, N. G. Impact craters in the northern hemisphere of Mars: Layered ejecta and central pit characteristics. Meteoritics & Planetary Science 41, 1425–1436 (2006).

Bruzzone, L. et al. RIME: Radar for Icy Moon Exploration. in 2013 IEEE International Geoscience and Remote Sensing Symposium - IGARSS (IEEE, 2013). doi:10.1109/igarss.2013.6723686.

Carrer, L. & Bruzzone, L. Automatic Enhancement and Detection of Layering in Radar Sounder Data Based on a Local Scale Hidden Markov Model and the Viterbi Algorithm. IEEE Transactions on Geoscience and Remote Sensing 55, 962–977 (2017).

Choudhary, P., Holt, J. W. & Kempf, S. D. Surface Clutter and Echo Location Analysis for the Interpretation of SHARAD Data From Mars. IEEE Geoscience and Remote Sensing Letters 13, 1285–1289 (2016).

Cofano, A. , Komatsu, G. , Pizzi, A. , Di Domenica, A. , Bruzzone, L. , Mitri, G. , Orosei, R.. Ganymede's Surface Investigation in Support of the Radar for Icy Moon Exploration (RIME) Instrument. (2015).

Croci, R., Seu, R., Flamini, E. & Russo, E. The SHAllow RADar (SHARAD) Onboard the NASA MRO Mission. Proceedings of the IEEE 99, 794–807 (2011).

Ferro, A. & Bruzzone, L. A novel approach to the automatic detection of subsurface features in planetary radar sounder signals. in 2011 IEEE International Geoscience and Remote Sensing Symposium (IEEE, 2011). doi:10.1109/igarss.2011.6049381.

Ferro, A. & Bruzzone, L. Automatic Extraction and Analysis of Ice Layering in Radar Sounder Data. IEEE Transactions on Geoscience and Remote Sensing 51, 1622–1634 (2013).

Ferro, A., Pascal, A. & Bruzzone, L. A Novel Technique for the Automatic Detection of Surface Clutter Returns in Radar Sounder Data. IEEE Transactions on Geoscience and Remote Sensing 51, 3037–3055 (2013).

Gerekos, C. et al. A Coherent Multilayer Simulator of Radargrams Acquired by Radar Sounder Instruments. IEEE Transactions on Geoscience and Remote Sensing 56, 7388–7404 (2018).

Grasset, O. et al. JUpiter ICy moons Explorer (JUICE): An ESA mission to orbit Ganymede and to characterise the Jupiter system. Planetary and Space Science 78, 1–21 (2013).

Grasset, O. et al. Review of Exchange Processes on Ganymede in View of Its Planetary Protection Categorization. Astrobiology 13, 991–1004 (2013).

Greenberg, R. Unmasking Europa. (Springer US, 2008). doi: 10.1007/978-0-387-09676-6

Des Marais, D. J. et al. The NASA Astrobiology Roadmap. Astrobiology 8, 715–730 (2008).

Heggy, E. , Paillou, P., Costard., F.,Mangold, N. , Ruffie, G., Demontoux, F., G. Grandjean, G.,and J. M. Malezieux. Local geoelectrical models of the Martian subsurface for shallow groundwater detection using sounding radars. Journal of Geophysical Research 108, (2003).

Heggy, E., Scabbia, G., Bruzzone, L. & Pappalardo, R. T. Radar probing of Jovian icy moons: Understanding subsurface water and structure detectability in the JUICE and Europa missions. Icarus 285, 237–251 (2017).

Horner, V. M. & Greeley, R. Pedestal craters on Ganymede. Icarus 51, 549–562 (1982).

Ilisei, A.-M., Khodadadzadeh, M., Ferro, A. & Bruzzone, L. An Automatic Method for Subglacial Lake Detection in Ice Sheet Radar Sounder Data. IEEE Transactions on Geoscience and Remote Sensing 57, 3252–3270 (2019).

Kjær, K. H. et al. A large impact crater beneath Hiawatha Glacier in northwest Greenland. Science Advances 4, eaar8173 (2018).

Legarsky, J. J., Gogineni, S. P. & Akins, T. L. Focused synthetic aperture radar processing of ice-sounder data collected over the Greenland ice sheet. IEEE Transactions on Geoscience and Remote Sensing 39, 2109–2117 (2001).

Thomas B. McCord, Gary B. H., Charles A. H. Hydrated Salt Minerals on Ganymede's Surface: Evidence of an Ocean Below. Science 292, 1523–1525 (2001).

Nunes, D. C. et al. Shallow Radar (SHARAD), pedestal craters, and the lost Martian layers: Initial assessments. Journal of Geophysical Research 116, (2011).

Orosei, R. et al. Radar evidence of subglacial liquid water on Mars. Science eaar7268 (2018). doi:10.1126/science.aar7268

Patterson, G. W. et al. Global geological mapping of Ganymede. Icarus 207, 845–867 (2010).

Sbalchiero, E. 3D simulations of the Radar for Icy Moon Exploration (RIME) data. MSc. Thesis, University of Trento (Italy).

Schenk, P. M. Morphology and scaling of ejecta deposits on icy satellites. Geophysical Research Letters 29, (2002).

Seu, R. et al. SHARAD: The MRO 2005 shallow radar. Planetary and Space Science 52, 157–166 (2004).

Showman, A. P., Malhotra, R. The Galilean Satellites. Science 286, 77–84 (1999).

Stuurman, C. M. et al. SHARAD detection and characterization of subsurface water ice deposits in Utopia Planitia, Mars. Geophysical Research Letters 43, 9484–9491 (2016).

Thakur, S. & Bruzzone, L. An Approach to the Simulation of Radar Sounder Radargrams Based on Geological Analogs. IEEE Transactions on Geoscience and Remote Sensing 1–19 (2019). doi:10.1109/tgrs.2019.2898027

Thakur, S., Vettor, A., Bruzzone, L. Analysis of subsurface hypotheses through simulation of RIME radargrams base on available analogous data. IEEE International Geoscience and Remote Sensing Symposium - IGARSS (accepted paper), (2019)

Zurek, R. W. & Smrekar, S. E. An overview of the Mars Reconnaissance Orbiter (MRO) science mission. Journal of Geophysical Research 112, (2007).

Websites

http://af-projects.it/sofa